On the stability of rotating stratified shear flow: An analytical study

Abdelaziz Salhi, Claude Cambon

On the stability of rotating stratified shear flow: An analytical study.

A. Salhi[1] & C. Cambon[2]

[1] *Département de Physique, Faculté des Sciences de Tunis, 1060, Tunis, Tunisia,*

[2] *Laboratoire de Mécanique des Fluides et d' Acoustique,*

Ecole Centrale de Lyon, UMR 5509, CNRS,

INSA, UCB, 69134 Ecully Cedex, France.

Abstract

We study the stability problem of unbounded shear flow, with velocity $U_i = S x_3 \delta_{i1}$, subjected to a uniform vertical density- stratification, with Brunt-Vaisala frequency N, and system rotation of rate Ω about an axis aligned with the spanwise (x_2) direction. The evolution of plane-wave disturbances in this shear flow is governed by a non-homogeneous second-order differential equation with time-dependent coefficients. An analytical solution is found to be described by Legendre functions in terms of the nondimensional parameter $\sigma_\varphi^2 = R(R+1)\sin^2\varphi + R_i$, where $R = (2\Omega/S)$ is the rotation number, φ is the angle between the horizontal wave vector and the streamwise axis and $R_i = N^2/S^2$ is the Richardson number. The long-time behavior of the solution is analyzed using the asymptotic representations of the Legendre functions. On the one hand, linear stability is analysed in terms of exponential growth, as in a normal mode analysis: the rotating stratified shear flow is stable if $R_i > 1/4$, or if $0 < R_i < 1/4$ and $R(R+1) > 0$ or if $R(R+1) < 0 < R(R+1) + R_i$ and $0 < R_i < 1/4$. It is unstable if $R_i < 0$ and $R(R+1)+R_i < 0$. On the other hand, different behaviors for the "exponentially stable" case can coexist in different wave-space regions: some modes undergo a power law growth or a power law decay, while other exhibit damped oscillatory behavior. For geophysical and astrophysical applications, stability diagrams are shown for all values of R_i, R and an arbitrary orientation of the wave vector. Crucial contributions to spectral energies are shown to come from the $k_1 = 0$ mode, which corresponds to an infinite streamwise wavelength. Accordingly, two-dimensional contributions to both kinetic and potential energies are calculated analytically in this streamwise direction.

1. INTRODUCTION

This study contributes to a general approach to turbulent flows subjected to mean, velocity and/or density, gradients and/or body forces. The mean flow studied here is a combination of pure plane shear of constant rate S, rotating along its spanwise direction with angular velocity Ω. An additional "stabilizing" vertical mean gradient of density, which results in a constant Brunt-Vaisala frequency N is considered. The mean flow is schematically shown in figure 1.

If one accept the simplification of no confinement, or no explicit effects of solid boundaries, this flow can be seen as a model for geophysical applications. At meso-scales, the local Coriolis parameter f, which replaces the system vorticity 2Ω, is almost constant, and usually small, but not negligeable, with respect to the frequency N which quantifies the local stable stratification. Stable stratification can be transient (inversion zone) or durable (tropopause, low stratosphere) in the atmosphere. It is durable in the ocean, at least near the thermocline and near the "deep pycnocline" (see, e.g., Pedlowski [1]). It can be shown that stably stratified zones mainly control the vertical turbulent mixing in atmosphere and ocean.

Without mean shear, the "vortex-wave" dynamics of three-dimensional rotating stratified flows is well documented, but its purely linear dynamic is poor, with essentially neutral modes, inertia-gravity wave modes and non-propagating quasi-geostrophic mode. The presence of a mean shear, such as thermal wind, jet-stream in tropopause, horizontal current in ocean, can dramatically alter vortex-wave dynamics, resulting in stabilizing more or in destabilizing the turbulent flow. Accordingly, the three external parameters S, f, N are all important in our dynamical study, with dimensionless combination such as $R^{-1} = R_0 = S/f$ (Rossby number) or $R_i = N^2/S^2$ (Richardson number). Another important instance of the model with all three (rotation, stratification, shear) ingredients is the case of thin, radially stratified accretion discs in astrophysics, where the angular momentum transport is central to their evolution. For instance, Johnson & Gammie [2] considered the nonaxisymmetric linear theory of radially stratified disks. They "worked in a shearing-sheet-like approximation, in which the vertical structure of the disk is neglected, and developed equations for the time evolution of a plane-wave perturbation comoving with the shear flow." They resolved analytically these equations considering an infinite wavelength in the spanwise direction (denoted here by $k_2 = 0$), for which the wave amplitudes are affected by shear and stratification

but not by rotation.

In the present study, we propose a complete linear stability analysis for the above base flow considering plane-wave disturbances with time-dependent wave vector $\boldsymbol{k}(t)$ ([3, 4]). We determine an analytical solution for the deterministic Green's function, in terms of a minimum number (2) of solenoidal components for the velocity disturbance field. We study its long-time behavior for an arbitrary orientation of the disturbance wave vector, not just for a special orientation that leads to a considerable simplification ([2]). This allows us to compute stability diagrams for all values of the rotation and Richardson numbers. Such stability diagrams are relevant for several geophysical and astrophysical applications. A sufficient condition for stability in bounded non-rotating stratified flows was demonstrated by Miles [5] to be $Ri > 1/4$ (see also Drazin & Reid [6]). In that analysis, the role of the inflectional point is essential, so that the stability of a rectilinear velocity profile, as in our present study, is a different problem; the value of $R_i = 1/4$, however, is recovered as a threshold value, as we will show further.

A short overview of the previous work which addresses the formalism of linear theory, which underlies both RDT and related stability analysis, is given in section 2.3. The essential common basis of these approaches, but also of nonlinear developments using them, is the deterministic Green's function, denoted g_{ij} here. The pure kinematic case (without buoyancy) is briefly discussed as follows: The equation for the disturbance in terms of a minimal number of solenoidal components can be written in Fourier space as

$$\dot{u}^{\alpha}(\boldsymbol{k}(t), t) + m_{\alpha\beta}(\boldsymbol{k}(t))u^{\beta}(\boldsymbol{k}, t) = f^{\alpha}(\boldsymbol{k}, t), \quad \alpha = 1, 2, \quad \beta = 1, 2, \tag{1}$$

in which the right-hand-side contains all nonlinear and/or forcing terms. Discarding the r-h-s in eq. (1), the linear solution calls into play the reduced Green's function, which links any realization of the fluctuating (or disturbance) field at time t to its initial counterpart at time t_0, so that

$$u^{(\alpha)}(\boldsymbol{k}(t), t) = g_{\alpha\beta}(\boldsymbol{k}(t), t)u^{(\beta)}(\boldsymbol{k}(t_0), t_0). \tag{2}$$

This *Green's function is deterministic* because randomness is only possibly introduced by the initial data $u_0^{(\beta)}$ in eq. (2). It is the unique ingredient needed to give a complete stability analysis, for instance, via a Floquet analysis of its eigenvalues when the time-dependent wave vector $\boldsymbol{k}(t)$ is periodic (e.g., [3, 4, 7–11]). In addition, linear operators are not systematically considered as dominant over the non-linear ones, as in conventional Rapid Distortion Theory

(RDT hereinafter), and the linear response is involved with stochastic nonlinear modeling (see, e.g., [12]). It is possible to incorporate the Green's function as a building block in fully nonlinear models and theories, in which nonlinear terms, more or less related to stochastic stirring forces, are treated as a source (f_α in the eq. (1)) in the right-hand-side of linearized equations, or

$$u^{(\alpha)}(\boldsymbol{k}(t), t) = g_{\alpha\beta}(\boldsymbol{k}(t), t)u^\beta(\boldsymbol{k}(t_0), t_0) + ...$$
$$+ \int_{t_0}^t g_{\alpha\beta}(\boldsymbol{k}(t'), t')f^\beta(\boldsymbol{k}(t'), t')dt'. \tag{3}$$

Simple instances of treating the "impulsional response" instead of the "initial-value response" of turbulence are given by Leprovost and Kim [13], in which the Reynolds stress tensor $\langle u_i u_j \rangle(t)$ resulting from a stirring term f_j with oversimplified (isotropic, white noise) spectrum is expanded in order to extract an effective viscous tensor. A similar "beta" term is sought in Magneto-Hydrodynamics, after the "alpha" one which is generally zero in the purely "hydro" case. A more sophisticated approach, in which the nonlinearity can be strong, is addressed by Rogachevskii [12].

Linearization of eq. (1), considered as an assumption (conventional RDT) or not [4], is discussed in subsection 2.3. Going back to the purely linear initial-value problem, *from now on in this article,* identification of the Green's function once and for all (e.g. [14]) allows us to predict second-order statistics, as in conventional RDT, but also gives access to higher order statistics, such as cubic moments [15, 16]. As mentioned before, in the linear case, randomness is only introduced by the initial data $u_0^{(\beta)}$, so that any n-th order moment at time t (in terms of velocity modes) can be derived from its initial counterpart using a tensorial product of n basic Green's function. As a first example, the history of turbulent kinetic energy $\mathcal{K}(t)$ can be found as

$$\mathcal{K}(t)/\mathcal{K}(t_0) = \int \int_{|\boldsymbol{k}(t_0)|=1} |\boldsymbol{g}|^2 \, d^2\boldsymbol{k}(t_0),$$

starting from isotropic initial data, so that the turbulent kinetic energy growth rate is directly linked to the norm of $\boldsymbol{g}$ (see, e.g., [8]). Considering the importance of elongated structures in the streamwise direction, such as streaks in the pure plane shear, and the importance of the two-dimensional Taylor-Proudman limit along the axis of rotation, we will restrict here the analytical calculation to statistical quantities that only involve the $k_1 = 0$ and $k_2 = 0$ modes. The related " two-dimensional energy components", defined below, were

shown to play an important role in the dynamics of large-scale motion in rotating (or) stratified sheared turbulence (see [17–19]). They correspond to the limit at $k_1 = 0$ (or at $k_2 = 0$) of the one-dimensional spectrum in term of the streamwise (spanwise) wavenumber, or equivalently, are the product of the integral length scales separated in the streamwise (or spanwise) direction $L_{ij}^{(1)}$ (or $L_{ij}^{(2)}$) by associated Reynolds stress components $\langle u_i u_j \rangle$,

$$\mathcal{E}_{ij}^{(1)}(t) = \pi \int_{k_1=0} \hat{R}_{ij}(\boldsymbol{k}, t) d^2 \boldsymbol{k} = L_{ij}^{(1)} \langle u_i u_j \rangle,$$

$$\mathcal{E}_{ij}^{(2)}(t) = \pi \int_{k_2=0} \hat{R}_{ij}(\boldsymbol{k}, t) d^2 \boldsymbol{k} = L_{ij}^{(2)} \langle u_i u_j \rangle, \tag{4}$$

in which $\hat{R}_{ij}(\boldsymbol{k}, t) \propto \langle \hat{u}_j^* \hat{u}_i \rangle$ denotes the three-dimensional spectral tensor and there is no summation on i, j. The dominance of the spectral components of $|k_1| \ll 1$ in the energy spectra and in the Reynolds stresses at large times has been discussed by Moffatt [14] for viscous pure shear flow and by Hanazaki & Hunt [18] for stably stratified shear flow. The spanwise two-dimensional energy components $\mathcal{E}_{ij}^{(2)}$ are also of interest, because $L_{11}^{(2)}$ gives the length scale for streaks spacing in the spanwise direction in pure plane shear, whereas the ratio $L_{11}^{(1)}/L_{11}^{(2)} = \mathcal{E}_{11}^{(2)}/\mathcal{E}_{11}^{(1)}$ gives the aspect ratio of streaklike structures in the pure plane shear flow, rotating or not [16, 17].) These spanwise two-dimensional energy components are not affected by system rotation, and correspond to the two-dimensional limit (Taylor-Proudman) with respect to the rotation axis, aligned with the spanwise direction of the mean shear here. As mentioned before, the analysis of Johnson & Gammie [2] focusses on these spectral contributions at $k_2 = 0$.

The paper is organized as follows. The basic equations for the base flow and the disturbances are given in §2. Conditions for validity of the linearization are addressed at the end of §2. Equations for the Fourier components of the disturbances in a local frame attached to the wave vector are given in §3. An analytical solution for the matrix g_{ij} at an arbitrary orientation of the wave vector is derived in §4. Section 5 deals with an exponential-growth stability analysis based on the long-time behavior of the trace of the matrix **g**. In section 6, some stability diagrams are presented, together with the long-time behavior of some modes, such as the ones associated to the pressure disturbance, and the streamwise and spanwise two-dimensional energy components. Section 7 presents our concluding remarks.

2. BASIC EQUATIONS

The fluid is assumed to be inviscid and nondiffusive. In the Boussinesq approximation, velocity and buoyancy fields $\tilde{\boldsymbol{u}}$ and $\tilde{b}$ are described by the following equations

$$\nabla \cdot \tilde{\boldsymbol{u}} = 0, \quad (\partial_t + \tilde{\boldsymbol{u}} \cdot \nabla)\tilde{\boldsymbol{u}} = -\nabla \tilde{p} - 2\boldsymbol{\Omega} \times \tilde{\boldsymbol{u}} + \tilde{b}\boldsymbol{n}, \tag{5}$$

$$(\partial_t + \tilde{\boldsymbol{u}} \cdot \nabla)\tilde{b} = 0, \tag{6}$$

where $\tilde{p}$ is a modified pressure (which includes the centrifugal acceleration potential divided by the fixed reference density ϱ_0, $\boldsymbol{n}$ denotes an upward vertical unit vector. The buoyancy term is proportional to the gravitational acceleration and to a density (for a liquid) or to a potential temperature (for a gas), and even to a scalar conscentration (salt). More general formulation is obtained in term of it, independently of the choice of the stratifying agent (temperature, salt) which allows the density to vary.

By taking the curl of the velocity equation in (5), we obtain the equation of the absolute vorticity $\tilde{\boldsymbol{\omega}} = \tilde{\boldsymbol{u}} + \boldsymbol{\Omega}$ (see, e.g. Greenspan [20]),

$$(\partial_t + \tilde{\boldsymbol{u}} \cdot \nabla)\,\tilde{\boldsymbol{\omega}} = \tilde{\boldsymbol{\omega}} \cdot \nabla \tilde{\boldsymbol{u}} + \nabla \times \left(\tilde{b}\boldsymbol{n}\right), \tag{7}$$

and we recover that, for inviscid and nondiffusive fluid, the Ertel (absolute) potential vorticity $\tilde{\Pi} = \tilde{\boldsymbol{\omega}} \cdot \nabla \tilde{b}$ (see, e.g. Pedlowski [1]) is a Lagrangian invariant, i.e.,

$$(\partial_t + \tilde{\boldsymbol{u}} \cdot \nabla)\tilde{\Pi} = 0. \tag{8}$$

As will be shown later, the above relation allows us to deduce a constant of motion for the disturbances to the base flow.

2.1. Base, or mean, flow

Decomposing the flow into a basic state and a disturbance, as $\tilde{\boldsymbol{u}} = \boldsymbol{U} + \boldsymbol{u}$, $\tilde{p} = P + p$, $\tilde{b} = B + b$, the basic state $\boldsymbol{U}, P, B$ consists of pure plane shear, with spanwise rotation and vertical stratification

$$U_i = Sx_3\delta_{i1}, \quad B = N^2 x_3, \quad \Omega_i = \Omega\delta_{i2}, \tag{9}$$

where N is the Brunt-Vaisala frequency and δ_{ij} is the Kronecker "delta" symbol. This frequency characterizes the strength of a stabilizing density gradient, with $N =$

$\sqrt{-\left(g/\varrho_0\right)\left(\partial\varrho/\partial x_3\right)}$ for instance in a liquid of mean density ρ varying linearly around a reference density ϱ_0. It follows that the basic absolute vorticity aligns with the spanwise axis, $\boldsymbol{W} = [0, S + 2\Omega, 0]^T$, and remains perpendicular to the buoyancy gradient, and hence, the base-flow Ertel potential vorticity is zero, $\Pi = 0$. Here, the superscript T denotes transpose.

2.2. Disturbances to the base flow

The above "linear" (velocity with respect to spatial coordinates) base flow is a particular solution of the Euler/Boussinesq equations (5-6), so that it is admissible according to Craik [4]. The equations for the disturbances to the base flow (9), in physical space are

$$\frac{\partial u_i}{\partial x_i} = 0,$$

$$\frac{d}{dt}\begin{pmatrix} u_1 \\ u_2 \\ u_3 \\ b \end{pmatrix} = \begin{bmatrix} 0 & 0 & -(S+2\Omega) & 0 \\ 0 & 0 & 0 & 0 \\ 2\Omega & 0 & 0 & 1 \\ 0 & 0 & -N^2 & 0 \end{bmatrix} \cdot \begin{pmatrix} u_1 \\ u_2 \\ u_3 \\ b \end{pmatrix} - \begin{pmatrix} \frac{\partial p}{\partial x_1} \\ \frac{\partial p}{\partial x_2} \\ \frac{\partial p}{\partial x_3} \\ 0 \end{pmatrix} - u_i\frac{\partial}{\partial x_i}\begin{pmatrix} u_1 \\ u_2 \\ u_3 \\ b \end{pmatrix}, \qquad (10)$$

where

$$\frac{d}{dt} = \frac{\partial}{\partial t} + Sx_3\frac{\partial}{\partial x_1}, \qquad \frac{\partial}{\partial x_i}\left(\frac{du_i}{dt}\right) = S\frac{\partial u_3}{\partial x_1}.$$

Due to the incompressibility constraint, the divergence of the above linear system of velocity equations yields the following Poisson equation for the pressure disturbance p:

$$-\nabla^2 p = \underbrace{2S\frac{\partial u_3}{\partial x_1} + 2\Omega\left(\frac{\partial u_3}{\partial x_1} - \frac{\partial u_1}{\partial x_3}\right) - \frac{\partial b}{\partial x_3}}_{linear\ part} + \underbrace{\frac{\partial u_j}{\partial x_i}\frac{\partial u_i}{\partial x_j}}_{nonlinear\ part}. \qquad (11)$$

Because $\tilde{\Pi} = \Pi + \varpi$ with $\Pi = 0$ as noted previously, equation (8) implies that

$$\varpi = \underbrace{(S+2\Omega)\frac{\partial b}{\partial x_2} + N^2\left(\frac{\partial u_2}{\partial x_1} - \frac{\partial u_1}{\partial x_2}\right)}_{linearized\ part} + \underbrace{\epsilon_{imn}\frac{\partial u_n}{\partial x_m}\frac{\partial b}{\partial x_i}}_{nonlinear\ part}, \qquad (12)$$

is also a Lagrangian invariant, for inviscid and nondiffusive fluid, or $d\varpi/dt = 0$ along trajectories. Here, ϵ_{imn} is the permutation tensor.

2.3. Conditions for validity of linearization

Before examining conditions for validity of linearization it is perhaps useful to give a short overview of the communities which address the formalism of linear theory.

First, in the turbulence community, the linear theory, or Rapid Distortion Theory (RDT) began with Batchelor & Proudman [21], with a focus on mean distortion induced by *irrotational* mean flows (linear flow with hyperbolic streamlines in the language of stability). Moffatt [14] was probably the first to concentrate on the pure plane shear (rectilinear streamlines), which presents much more interest for the whole theory of turbulent shear flow. This way was followed by Townsend, in the revised version of his book [22]. Finally efforts were made towards RDT studies for rotating shear [17, 23] and stratified shear [18], but *separately considered.*

Second, a new impulse to the theory arose when Pierrehumbert [24] characterized the elliptical flow instability by a classical normal-mode analysis, whereas Bayly [3] used the same year a simpler and more elegant method which was nothing other than the base of RDT. The general case of RDT applied to elliptical, rectilinear and hyperbolic flows in a rotating frame is addressed in [8], reconciling RDT and stability analysis. Many studies followed the Bayly's one in the hydrodynamic community, using "exact solutions for disturbances to linear flows in terms of Kelvin modes", or in terms of *advected* Fourier modes with time-dependent wavevector.

A third community can be identified, with main applications in astrophysics. The linear response of turbulence to various effects of shear, density-stratification and rotation is used for a better modelisation of the turbulence in accretion disks, mainly (see, e.g. [2, 13]). Analogies and partial balance between (self)-gravitational, centrifugal, and buoyancy forces are studied, not to mention the Lorentz force in the important context of the magneto-rotational instability.

It is important to stress that these communities often publish in different journals and use different parlance and jargons. For instance, the basic Fourier mode with time-dependent wave-vector is called a "Kelvin mode" in the second community and a "shear-wave" or "shwave" in the third one.

From the viewpoint of Craik [4], for instance, linearization is not even considered as an assumption: The admissible base flow is shown to be compatible with the wavelike form (13)

for the disturbance flow, and the superposition of both is called "a class of exact solutions" for Euler equations. As said before, this is nothing other than a formal rediscovery of RDT, but one in which nonlinearity is rigorously excluded in the equations for the disturbance flow: Only *single-mode* perturbation is considered and nonlinearity is zero for a single Fourier mode in the incompressible case. We think that it is more physical to consider an actual disturbance field as a superposition of many Fourier modes, so that the initial condition is characterized by a dense energy spectrum. Prediction of statistics from the RDT solution for the initial-value problem reintroduces the problem of evaluating nonlinear terms mediated by interacting Fourier modes. The fact that the mean (or base) flow is only characterized by spatial gradients (e.g. of magnitude S) has important consequences. First, it is not possible to define a length scale and a velocity scale for the base flow, but only a time scale (e.g. S^{-1}). This explains why linearization is not justified, as in conventional linear-stability analysis, by a —small— ratio of disturbance-to-base-velocity scale, but by an assumption of small elapsed time. The linear solution is expected to hold for small St only, but the maximum St at which it is valid depends crucially on the initial shear-rapidity factor SL/u', where L and u' are typical length and velocity scales for the disturbance flow: SL/u' gives a rough statistical estimate of the ratio of linear term to nonlinear one. Previous direct numerical simulations (DNS) studies of homogeneous rotating or stratified sheared turbulence with sufficiently strong shear rate show that the mean-shear turbulence interactions dominate the turbulence-turbulence interactions and the linear theory well predicts ratios of energies and normalized fluxes that characterize the anisotropy of the large scales motion [17, 18, 25–27]. However, in some extreme unsheared flow cases, like rotating turbulence with angular velocity Ω and low Rossby number $Ro = u'/(2\Omega L)$, the nonlinearity becomes significant only after a very long time, such as $\Omega t = Ro^{-2}$. This is essentially explained by the depletion of nonlinearity that is due to phase mixing by dispersive inertial waves at small Rossby number. Another example is the case of stably stratified turbulence: Linearity is expected to be valid at low Froude number for reasonable values of Nt. This is wrong, because a part of the motion, the toroidal velocity component, does not scale with the Froude number at small Froude number, as the poloidal component does, so that an important nonlinear term restricted to the toroidal flow is present, even at short time. In short, only a refined evaluation of the nonlinear term, and/or a comparison between RDT and DNS, can delineate the parametric domain in which the linear assumption is relevant.

3. PLANE WAVES DISTURBANCES

3.1. The equations for the Fourier components

As the starting point of RDT-like stability analysis, individual modes are expressed in terms of Fourier modes with time-dependent wave vector

$$[\boldsymbol{u}(\boldsymbol{x},t), p(\boldsymbol{x},t), b(\boldsymbol{x},t)] = \left[\hat{\boldsymbol{u}}(t), \hat{p}(t), \hat{b}(t)\right] \exp\left(\imath \boldsymbol{k}(t){\cdot}\boldsymbol{x}\right). \tag{13}$$

The wave vector $\boldsymbol{k}$ satisfies the (eikonal-type) equation : $dk_i/dt = -\left(\partial U_j/\partial x_i\right)k_j$, with solution [14]

$$k_1 = K_1 \quad k_2 = K_2, \quad k_3(t) = K_3 - k_1 St, \tag{14}$$

in which the capital letter denotes initial value $(\boldsymbol{k}(t_0)$ in eq. (2).) Accordingly, from the Poisson equation (eq. (11)), we deduce the expression of the Fourier mode $\hat{p}$,

$$\hat{p} = \frac{\imath}{k^2}\left[2\left(S+\Omega\right)k_1\hat{u}_3 - 2\Omega k_3\hat{u}_1 - k_3\hat{b}\right], \tag{15}$$

and the differential system (10) is transformed as follows

$$\frac{d}{dt}\begin{pmatrix} \hat{u}_1 \\ \hat{u}_2 \\ \hat{u}_3 \\ \hat{b} \end{pmatrix} = \begin{bmatrix} 0 & 0 & -(S+2\Omega) & 0 \\ 0 & 0 & 0 & 0 \\ 2\Omega & 0 & 0 & 1 \\ 0 & 0 & -N^2 & 0 \end{bmatrix} {\cdot} \begin{pmatrix} \hat{u}_1 \\ \hat{u}_2 \\ \hat{u}_3 \\ \hat{b} \end{pmatrix} - \imath\hat{p}\begin{pmatrix} k_1 \\ k_2 \\ k_3 \\ 0 \end{pmatrix}, \tag{16}$$

with the incompressibility constraint $\hat{\boldsymbol{u}}{\cdot}\boldsymbol{k} = 0$ implied. In addition, the fact that the disturbance of the Ertel potential vorticity ϖ (see eq. (12)) is a Lagrangian invariant, $d\varpi/dt = 0$, implies that the Fourier mode $\hat{\varpi}$ is a constant of motion, or

$$-\imath\hat{\varpi}(t) = -\imath\varpi(\boldsymbol{x},t)\exp(-\imath\boldsymbol{k}(t){\cdot}\boldsymbol{x}) = N^2\left(k_1\hat{u}_2 - k_2\hat{u}_1\right) + (S+2\Omega)k_2\hat{b} = \text{constant}. \tag{17}$$

Discarding a priori the simple case of purely vertical wavevector $(k_1 = k_2 = 0)$, in which a simple algebraic growth (linear in t) is found, we consider in the following that the squared amplitude of the wave number in the horizontal plane, $k_h^2 = k_1^2 + k_2^2$, is not zero and we set $k_1 = k_h\cos\varphi$ and $k_2 = k_h\sin\varphi$. Therefore in view of equations (15), (17) and the incompressibility constraint, the system (16) reduces to a rank 2 differential system.

3.2. Poloidal, toroidal and potential modes

An alternative way which reduces the number of components is to use a local frame in which the incompressibility constraint is satisfied by construction. In addition, effects of shear, rotation and stratification are more physically reflected in this frame, in which dispersion frequencies directly appear (see [16] and subsequent eqs. (20-22).) This frame coincides with the horizontal fixed frame if $\boldsymbol{k}$ is vertical ($\boldsymbol{k} \parallel \boldsymbol{n}$) , and otherwise is defined by

$$\boldsymbol{e}^{(1)} = \boldsymbol{k} \times \boldsymbol{n}/\|\boldsymbol{k} \times \boldsymbol{n}\|, \quad \boldsymbol{e}^{(2)} = \boldsymbol{k} \times \boldsymbol{e}^{(1)}/k, \quad \boldsymbol{e}^{(3)} = \boldsymbol{k}/k,$$

so that $\hat{\boldsymbol{u}}$ has only two components, $\hat{\boldsymbol{u}} = u^{(1)}\boldsymbol{e}^{(1)} + u^{(2)}\boldsymbol{e}^{(2)}$. Here, $\boldsymbol{n}$ is the upward vertical unit vector ($n_i = \delta_{i3}$), and hence,

$$\boldsymbol{e}^{(1)} = [\sin\varphi, \ -\cos\varphi, \ 0]^T, \quad \boldsymbol{e}^{(2)} = \left[\frac{k_3}{k}\cos\varphi, \ \frac{k_3}{k}\sin\varphi, \ -\frac{k_h}{k}\right]^T, \quad k_1 = k_h\cos\varphi, k_2 = k_h\sin\varphi \tag{18}$$

so that $\boldsymbol{e}^{(1)}$ is a time-independent unit vector, whereas k_3, k, and therefore $\boldsymbol{e}^{(2)}$ remain time-dependent via eq. (14.) If $k_h = |\boldsymbol{k} \times \boldsymbol{n}| \neq 0$, the two components $u^{(1)}$ and $u^{(2)}$ correspond to toroidal and poloidal velocity components in physical space [16]. On the other hand, the limit of pure vertical wave vectors gives the vertically sheared horizontal flow (VSHF, see [16, 28]), a particular mode of motion which is very important in the stratified flow case. Finally and for consistency, the third dependent variable $\hat{b}$ is scaled to have the same dimension as the velocity modes, or

$$u^{(3)} = -\frac{\hat{b}}{N}, \tag{19}$$

so that the spectral density of total (kinetic + potential) energy is $u^{(1)*}u^{(1)} + u^{(2)*}u^{(2)} + u^{(3)*}u^{(3)}$, where the asterix denotes complex conjugate. As shown in Appendix 1, the transformation of system (16) into the local frame yields

$$\frac{d}{dt}\begin{pmatrix} u^{(1)} \\ u^{(2)} \\ u^{(3)} \end{pmatrix} + \begin{bmatrix} 0 & -\sigma_r - S\frac{k_2}{k} & 0 \\ \sigma_r & -S\frac{k_3 k_1}{k^2} & -\sigma_s \\ 0 & \sigma_s & 0 \end{bmatrix}\begin{pmatrix} u^{(1)} \\ u^{(2)} \\ u^{(3)} \end{pmatrix} = 0, \tag{20}$$

in which

$$\sigma_r = 2\Omega\frac{k_2}{k} = 2\Omega\frac{k_h}{k}\sin\varphi \tag{21}$$

11

and

$$\sigma_s = N \frac{k_h}{k} \tag{22}$$

are the dispersion frequency of inertial and gravity waves, respectively. All the characteristic frequencies and typical coupling of the physical system are then displayed in the matrix. As for the constant of motion in eq. (17), it can be rewritten as

$$k\sigma_s u^{(1)} + (k\sigma_r + k_h S \sin \varphi) u^{(3)} = \text{constant}, \tag{23}$$

and can be also recovered by combining the first and the third lines in system (20). Relation (23) generalizes the conservation of the toroidal velocity component, sometime called the "purely vortex mode", without shear and without rotation. The first term in the l-h-s of eq. (23) corresponds to vertical vorticity (fluctuating vorticity projected on the direction of the mean gradient of buoyancy), whereas the second term corresponds to the scalar product of mean absolute vorticity by the gradient of fluctuating buoyancy.

4.   THE REDUCED GREEN FUNCTION

In this section we will derive a complete solution for the reduced Green function. In term of this three-mode (toroidal, poloidal, potential) vector, the reduced Green function g_{ij} $(i, j = 1, 2, 3)$ such that

$$u^{(i)}(\boldsymbol{k}(t), t) = g_{ij}(\boldsymbol{k}, t, 0) u^{(j)}(\boldsymbol{K}, 0), \tag{24}$$

is introduced, as its pure kinematic counterpart in eq. (2). It is governed by the same equation as $u^{(i)}$ is, but with universal initial condition $\mathbf{g}(0) = \mathbf{I}_3$, where $\mathbf{I}_3$ is the 3×3 unit matrix. In order to display the minimum of nondimensional terms, g_{3j} is subsituted to $(S/N)g_{3j}$, and $\tau = St$ is a non-dimensional time. This amounts to replace (19) by

$$u^{(3)} = -\frac{S}{N^2} \hat{b}, \tag{25}$$

and therefore to recover a R_i-weighted potential energy. For the sake of clarity, we give here the differential system for g_{ij},

$$\frac{d\mathbf{g}}{d\tau} + \mathbf{m} \cdot \mathbf{g} = \mathbf{0}, \tag{26}$$

where

$$m_{ij} = \frac{1}{S} \begin{bmatrix} 0 & -\sigma_s - S\frac{k_2}{k} & 0 \\ \sigma_r & -S\frac{k_1 k_3}{k^2} & -\frac{N}{S}\sigma_s \\ 0 & \frac{S}{N}\sigma_s & 0 \end{bmatrix} = \begin{bmatrix} 0 & -(1+R)\frac{k_2}{k} & 0 \\ R\frac{k_2}{k} & -\frac{k_1 k_3}{k^2} & -\frac{k_h}{k}R_i \\ 0 & \frac{k_h}{k} & 0 \end{bmatrix} \tag{27}$$

which displays the two important nondimensional numbers

$$R = 2\Omega/S, \quad R_i = N^2/S^2, \tag{28}$$

namely the rotation number and the Richardson number, respectively.

It is important to point out that the solution for **g** *cannot be derived from diagonalizing* **m** *and using exponentiation, because the coefficients are time-dependent via $k_3(t)$ and $k(t)$ in eq. (27) from eq. (14), so that eigenvectors of* **m** *are time-dependent too. Only in the case $k_1 = 0$, diagonalizing the matrix is sufficient for solving the problem.*

Similarly, the constant of motion in eq. (23) can be rewritten in terms of the reduced Green function as

$$g_{1j} + [(1+R)\sin\varphi]g_{3j} = \delta_{1j} + [(1+R)\sin\varphi]\delta_{3j}, \tag{29}$$

and the relation

$$\frac{1}{k}\frac{dk}{d\tau} = -\frac{k_1 k_3}{k^2}, \tag{30}$$

is deduced from the equ. (14). Using eqs. (26), (27), (29) and (30), the equations for g_{2j} and g_{3j} $(j = 1, 2, 3)$ can be rewritten as

$$\frac{d}{d\tau}[(k/k_h)g_{2j}] = \sigma_\varphi^2 g_{3j} - [\delta_{1j} + \delta_{3j}(R+1)\sin\varphi]R\sin\varphi, \tag{31}$$

$$\left(k^2/k_h^2\right)\frac{d}{d\tau}g_{3j} = -(k/k_h)g_{2j}, \tag{32}$$

where

$$\sigma_\varphi^2 = R(R+1)\sin^2\varphi + R_i, \quad \sigma_\varphi^2(\pi \pm \varphi) = \sigma_\varphi^2(\varphi). \tag{33}$$

Given the symmetries of $\sin^2\varphi$, we only consider the modes $0 \le \varphi \le \pi/2$.

4.1. Case where $\sigma_\varphi^2 = 0$

When $\sigma_\varphi^2 = 0$, or equivalently, $R(R+1)\sin^2\varphi + R_i = 0$, the integration of equation (31) with the initial conditions $g_{2j}(0) = \delta_{2j}$, yields

$$g_{21} = (k_h/k)(R\sin\varphi)\tau, \quad g_{22} = K/k, \quad g_{23} = -R_i(k_h/k)\tau. \tag{34}$$

13

Substituting the above solution into (32) and integrating, we obtain

$$g_{33} = 1 - \frac{K_3}{k_h} \frac{R_i}{\cos^2 \varphi} \left[\frac{K_3}{k_h} \left(\arctan \frac{k_3}{k_h} - \arctan \frac{K_3}{k_h} \right) + \log \frac{K}{k} \right],$$

$$g_{31} = \frac{(g_{33} - 1)}{[(R+1) \sin \varphi]}, \quad g_{32} = \frac{K}{k_1} \left(\arctan \frac{k_3}{k_h} - \arctan \frac{K_3}{k_h} \right). \tag{35}$$

Also, the substitution of the later solution into relation (29) allows us to deduce the expression of g_{1j} $(j = 1, 2, 3)$. For instance,

$$g_{11} = 1 - [(R+1) \sin \varphi] \, g_{31} = 2 - g_{33}. \tag{36}$$

The above solutions show that all components g_{ij} do not have the same long-time behavior. For instance, at $k_1 \neq 0$, g_{22} approaches zero for long times, while g_{21} approaches a non-zero constant value. On the other hand, it will be shown in the next section 5 that the exponential growth is only characterized by the first invariant, or the trace of $\mathbf{g}$. Accordingly, we will perform the stability analysis in the next section in term of exponential growth firstly, as in a normal mode stability analysis, putting aside the multifold "componentality" of $\mathbf{g}$ which characterize the exponentially "stable" case.

4.2. Case where $\sigma_\varphi^2 \neq 0$

When $\sigma_\varphi^2 \neq 0$, the second-order differential equations that can be derived from equations (31) and (32) are

$$\frac{d^2}{d\tau^2} \left[(k/k_h) \, g_{2j} \right] + \sigma_\varphi^2 g_{2j} = 0, \tag{37}$$

$$\frac{d}{d\tau} \left(\frac{k^2}{k_h^2} \frac{dg_{3j}}{d\tau} \right) + \sigma_\varphi^2 g_{3j} = R \sin \varphi \left[\delta_{j1} + \delta_{j3} (R+1) \sin \varphi \right]. \tag{38}$$

While, in the present study, we resolve equation (38) for any orientation of the wave vector, equ. (37) is reported here in order to note similarities between the present study and previous work by Johnson & Gammie [2]. The vertical mode $\hat{u}_3$ and the poloidal mode $u^{(2)}$ are related by

$$\hat{u}_3 = u^{(2)} e_3^{(2)} = -(k_h/k) u^{(2)} = -(k_h/k) g_{2j} u_0^{(j)}. \tag{39}$$

Accordingly, the equation for $\hat{u}_3$ is derived from (31) as

$$\frac{d^2}{d\tau^2} \left[\left(k^2/k_h^2 \right) \hat{u}_3 \right] + \sigma_\varphi^2 \hat{u}_3 = 0, \tag{40}$$

14

which is the same as equation (56) in Johnson & Gammie [2], up to a different notation. As indicated previously, Johnson & Gammie resolved the later equation for an infinite spanwise wavelength, or $k_2 = 0$, $\varphi = 0$. For this particular orientation of the wave vector, the coefficient σ_φ^2 reduces to the Richardson number, $\sigma_\varphi^2 = R_i$, and the reduced Green function does not depend on rotation number. Of course $k_2 = 0$ is also the two-dimensional manifold for which the Coriolis effect vanishes, as vanishes the dispersion frequency of inertial waves in (21-22).

The particular solution of equation (38) is time independent,

$$g_{3j}^p = \frac{R \sin \varphi}{\sigma_\varphi^2} \left(\delta_{j1} + \delta_{j3} \left(R + 1 \right) \sin \varphi \right), \quad (j = 1, 2, 3). \tag{41}$$

In order to resolve the associated homogeneous equation, we first consider the case where $k_1 = 0$ (i.e., $\varphi = \pi/2$).

The $k_1 = 0$ mode

At $k_1 = 0$ or $\varphi = \pi/2$, the wave vector is no longer time-dependent, with $k_2 = K_2$ and $k_3 = K_3$), and hence, the coefficient k^2/k_h^2 in equation (38) becomes constant too. In that case, all the elements of the matrix $\mathbf{g}$ have the same behavior (for the sake of clarity, the expression of the solution at $k_1 = 0$ is reported in Appendix),

$$g_{ij} \propto \exp \left[\pm \imath (k_h/k) \tau \sqrt{\sigma_\varphi^2} \right] = \exp \left[\pm \imath (k_h/k) \tau \sqrt{R(R+1) + R_i} \right], \tag{42}$$

indicating exponential growth when $R(R+1) + R_i < 0$ and an oscillatory behavior when $R(R+1) + R_i > 0$. In the later case, there are inertia-gravity-shear waves propagating in the $k_1 = 0$ plane ($\sim \exp \imath \left(k_2 x_2 + k_3 x_3 - \omega t \right)$ with frequency, $\omega = S(k_h/k)\sqrt{R(R+1) + R_i}$. The phase velocity $\mathbf{V}_\phi$ and the group velocity $\mathbf{V}_g = \nabla_{\mathbf{k}} \omega$ (see e.g., [20]) are perpendicular ($\mathbf{V}_\phi \cdot \mathbf{V}_g = 0$) and have the same modulus, $V_g = V_\phi = \omega/k$.

Case where $k_1 \neq 0$

When $k_1 \neq 0$, the use of the pure imaginary variable, $z = \imath k_3/k_h = \imath \left(K_3/k_h \right) - \imath \tau \cos \varphi$, transforms the homogeneous equation (associated to (38)) as

$$\frac{d}{dz} \left[\left(1 - z^2 \right) \frac{d}{dz} g_{3j} \right] + \mu(1 + \mu) g_{3j} = 0, \tag{43}$$

15

where the coefficient μ takes the form

$$\mu = \frac{1}{2}\left[-1 + \sqrt{1 - 4\sigma_\varphi^2/\cos^2\varphi}\right], \tag{44}$$

depending on the parameter R and R_i and on the azimuthal angle φ, or equivalently, on the horizontal wave vector $\boldsymbol{k}_h = \boldsymbol{k} - k_3\boldsymbol{e}_3$. The role of the coefficient μ in characterizing the flow stability will be addressed in the next section. For instance, we note that equation (43) has two linearly independent solutions: $P_\mu(z)$ and $Q_\mu(z)$ that are called Legendre functions of the first and second kind respectively (see [29, 30]). The expression of the components g_{ij} in terms of Legendre functions are given in Appendix for the sake of clarity. We note that the solutions found by Hanazaki & Hunt [18] in the non-rotating stratified shear case $(R = 0)$ and those by Salhi [23] in the non-stratified rotating shear $(R_i = 0)$ are recovered. Furthermore, because the Legendre functions can be expressed in terms of hypergeometric functions (see e.g., [29, 30]), the solutions found by Johnson & Gammie [2] for an infinite spanwise wavelength (i.e., $\varphi = 0$) in the case of radially stratified shearing disks (see their equations (66)-(69)) and those found by Salhi & Cambon [17] for the rotating shear case (see their Appendix) can also be recovered.

5. STABILITY ANALYSIS

In this section, we demonstrate that, in terms of exponential growth, as for a normal mode analysis, there is instability when $\sigma_\varphi^2 < 0$. The modes φ for which $\sigma_\varphi = 0$ are neutral, while those for which $\sigma_\varphi^2 > 0$ are stable.

5.1. Characteristic invariants for the reduced Green function

It is demonstrated that the stability problem can be characterized by the unique unknow $trace\ \mathbf{g} = g_{11} + g_{22} + g_{33}$ which is the first invariant of $\mathbf{g}$. The reduced Green function has three eigenvalues, say λ_1, λ_2 and λ_3. Because there is a constant of motion, in eq. (23), which can be rewritten as $\mathbf{g}^T{\cdot}\boldsymbol{\psi} = \boldsymbol{\psi}$ where $\boldsymbol{\psi} = [1, 0, (1+R)\sin\varphi]^T$, one of the eigenvalue of $\mathbf{g}$ is therefore equal to 1, say $\lambda_1 = 1$. Accordingly, the invariants of $\mathbf{g}$ are only characterized by λ_2 and λ_3: the trace is equal to the sum of eigenvalues, and the determinant is equal to their product, so that

$$trace\ \mathbf{g} = 1 + \lambda_2 + \lambda_3, \quad Det\ \mathbf{g} = \lambda_2\lambda_3. \tag{45}$$

16

The link of λ_2 and λ_3 to the trace eventually comes from the analytical derivation of the determinant,

$$Det \; \mathbf{g} = \frac{K}{k}, \tag{46}$$

which is a classical result for shear flows [8, 10]. Because the sum of the two non-trivial eigenvalues is $trace \; \mathbf{g} - 1$ and their product is K/k, they are the roots of the algebraic equation $\lambda^2 - (trace \; \mathbf{g} - 1) \, \lambda + K/k = 0$, and therefore are given by

$$\lambda_2 = \frac{1}{2} \left[(trace \; \mathbf{g} - 1) + \sqrt{(trace \; \mathbf{g} - 1)^2 - 4\frac{K}{k}} \right], \quad \lambda_3 = (K/k)(1/\lambda_2), \tag{47}$$

in which the only unknown is the trace of $\mathbf{g}$. The proof of eq. (46) is easyly reminded as follows. From eqs. (26) and (27) is found

$$\frac{d}{dt} Det\mathbf{g} = m_{ii} Det\mathbf{g},$$

with $m_{ii} = k_1 k_3 / k_2$. Because

$$k\frac{dk}{dt} = k_i \frac{dk_i}{dt} = -k_i \frac{\partial U_j}{\partial x_i} k_j = -S k_1 k_2,$$

$m_{ii} = -(1/k)dk/dt$ and $d/dt \, (kDet \; \mathbf{g}) = 0$ with $Det \; \mathbf{g}(\boldsymbol{k}, 0) = 1$, QED.

5.2. Unstable, neutral and stable modes

When $\sigma_\varphi^2 = 0$, we deduce from the solutions (34)-(36) in §4.1 that

$$trace \; \mathbf{g} = g_{11} + g_{22} + g_{33} = 2 + K/k. \tag{48}$$

The substitution of the later expression into the first equation in (47) yields $\lambda_2 = 1$, so that $\lambda_3 = K/k$, where $\lambda_1 = 1$. Because $\lim_{\tau \to \infty} K/k = 0$, the modes φ for which $\sigma_\varphi^2 = 0$, are then neutral in terms of a normal mode analysis.

When $\sigma_\varphi^2 \neq 0$ and $k_1 = 0$ (i.e., $\varphi = \pi/2$), one has $\lambda_1 = 1$, $\lambda_2, \lambda_3 = \exp \left[\pm \imath (k_h/k) \tau \sqrt{R(R+1) + R_i} \right]$ (see equation (42)), and hence, there is an exponential instability for $\sigma_\varphi^2 = R(R+1) + R_i < 0$.

When $\sigma_\varphi^2 \neq 0$ and $k_1 \neq 0$, the expression of $trace \; \mathbf{g}$ is found as (see Appendix),

$$trace \; \mathbf{g} = 1 + \left(1 - z_0^2\right) \left[Q_\mu'(z_0) P_\mu(z) - P_\mu'(z_0) Q_\mu(z) - \left[\frac{1 - z^2}{1 - z_0^2} \right]^{1/2} \left(Q_\mu(z_0) P_\mu'(z) - P_\mu(z_0) Q_\mu'(z) \right) \right], \tag{49}$$

17

where the prime denotes differentiation with respect to the complex variable z and $z_0 = z(0) = K_3/k_h = \imath \cot\theta$. In order to analyze the long time behavior of *trace* $\mathbf{g}$ we use the asymptotic representations of the Legendre functions (see [29] p. 1011, Eq. 8.776),

$$P_\mu(z) = \frac{2^\mu}{\sqrt{\pi}} \frac{\Gamma(\mu+1/2)}{\Gamma(\mu+1)} z^\mu + \frac{\sqrt{\pi}}{2^{(\mu+1)}} \frac{\Gamma(\mu+1)}{\Gamma(\mu+3/2)} z^{-\mu-1},$$

$$Q_\mu(z) = \frac{\sqrt{\pi}}{2^{(\mu+1)}} \frac{\Gamma(\mu+1)}{\Gamma(\mu+3/2)} z^{-\mu-1},$$

where $2\mu \neq \pm 1, \pm 2, \pm 3, ...$ and $\Gamma(z)$ denotes the gamma function. The substitution of the later relations into (49) yields

$$trace\ \mathbf{g} = 1 + D_1 z^\mu + D_2 z^{-1-\mu}, \quad 2\mu \neq \pm 1, \pm 2, ..., \tag{50}$$

where

$$D_1 = \frac{2^\mu}{\sqrt{\pi}} \frac{\Gamma(\mu+1/2)}{\Gamma(\mu+1)} \left(1 - z_0^2\right) \left[Q'_\mu(z_0) + \imath \frac{\mu}{\sqrt{1-z_0^2}} Q_\mu(z_0) \right]$$

$$D_2 = \frac{\sqrt{\pi}}{2^{(\mu+1)}} \frac{\Gamma(\mu+1)}{\Gamma(\mu+3/2)} \left(1 - z_0^2\right) \left[Q'_\mu(z_0) - P'_\mu(z_0) + \imath \frac{\mu+1}{\sqrt{1-z_0^2}} \left(Q_\mu(z_0) - P_\mu(z_0)\right) \right].$$

In view of equation (45) it is useful to calculate $|trace\ \mathbf{g} - 1|^2$

$$|trace\ \mathbf{g} - 1|^2 = |D_1|^2 |z^\mu|^2 + |D_2|^2 |z^{-1-\mu}|^2 + 2\Re\left[D_1 D_2^\star z^\mu \left(z^{-1-\mu}\right)^\star \right]. \tag{51}$$

When $\sigma_\varphi^2 < 0$, the coefficient μ (see equation (44)) is real of positive sign, $\mu > 0$. In that case, the modulus of the eigenvalues of λ_2 and λ_3 behave like,

$$|\lambda_2| \sim (\tau \cos\varphi)^\mu > |\lambda_3| \sim (\tau \cos\varphi)^{-1-\mu}, \tag{52}$$

since $-(1+\mu) < -1/2 < \mu$ and $K/k \sim (\tau \cos\varphi)^{-1}$ for long times. This signifies that, when $\sigma_\varphi^2 < 0$, there is an algebraic growth for $k_1 \neq 0$ and an exponential growth at $k_1 = 0$.

When $\sigma_\varphi^2 > 0$, we distinguish two cases. The first case is characterized by $0 < \sigma_\varphi^2 < (\cos^2\varphi)/4$. In that case, the coefficient μ is real of negative sign, $-1/2 < \mu < 0$, and $|\lambda_2|, |\lambda_3|$, which are also described by equation (52), undergo a power law decay. The second case is characterized by $\sigma_\varphi^2 > (\cos^2\varphi)/4$. In that case, the coefficient μ is complex, $\mu = -1/2 + \imath\Im\mu$, where

$$\Im\mu = \frac{\sqrt{4\sigma_\varphi^2 - \cos^2\varphi}}{2\cos\varphi}, \tag{53}$$

18

and equation (51) can be rewritten as follows

$$|\text{trace }\mathbf{g} - 1|^2 = [\tau\cos\varphi]^{-1}\left[A + r_0\cos\left(\Im\mu\log\left(\tau\cos\varphi\right) + \beta\right)\right], \tag{54}$$

where

$$A = |D_1|^2\,\mathrm{e}^{-\pi\Im\mu} + |D_2|^2\,\mathrm{e}^{\pi\Im\mu}, \quad 2D_1 D_2^* = r_0\mathrm{e}^{\imath\beta}.$$

This implies that $|\lambda_2|$ (respectively, $|\lambda_3|$) behaves like $(\tau\cos\varphi)^{-1/2}$ (respectively, $(\tau\cos\varphi)^{-3/2}$). Furthermore, by setting $y = \log(\tau\cos\varphi)$, equation (54) becomes

$$|\text{trace }\mathbf{g} - 1|^2 = \mathrm{e}^{-y}\left[A + r_0\cos\left(\Im\mu\ y + \beta\right)\right].$$

Therefore, $|\text{trace }\mathbf{g} - 1|^2$ versus y exhibits a damped oscillatory behavior with period $Y = 2\pi/\Im\mu$. For this, the modes for which $\sigma_\varphi^2 > (\cos^2\varphi)/4$ can be called the modes with "damped oscillatory" behavior.

6. DISCUSSION

In this section, we compute stability diagrams for all values of the rotation and Richardson numbers. These diagrams would be relevant for several geophysical, astrophysical and industrial applications. For instance, the stability condition of Keplerian disks with modest radial gradients is expected to be $|R_i| \ll 1$ [2]. In addition, we give the long-time behavior of Fourier modes associated to the velocity, pressure, and density disturbances. Because in sheared flows with or without rotation or stratification, the mode $k_1 = 0$, which corresponds to an infinite wavelength in the streamwise direction, plays an important role in the dynamics of large-scales motion ([14, 17–19, 25]), the related streamwise "two-dimensional energy components", are addressed at the end of this section.

6.1. Stability diagrams

In the $(R(R+1), R_i)$ plane, the relation $\sigma_\varphi^2 = 0$, which characterizes the neutral modes,

$$R(R+1)\sin^2\varphi + R_i = 0,$$

defines straightlines that intersect at the point $O(0,0)$. Each one of these straightlines divides the $(R(R+1), R_i)$ plane into two regions. the upper region characterizes stability while the

lower one characterizes instability as will be shown now. Two of these straightlines are represented in figure 2. The first one corresponds to a zero value of the azimuthal angle (i.e., $\varphi = 0$, or equivalently, the $R(1+R)$ axis), while the second one, which is labelled by (d_2), corresponds to an arbitrary value of the azimuthal angle (i.e., $0 < \varphi < \pi/2$).

When φ varies between 0 and $\pi/2$, there are domains in the $(R(R+1), R_i)$ plane for which modes with different behaviors can coexist as explained as follows. For the region defined by (i.e., the region (IV) in figure 3),

$$0 < R_i < 1/4 \quad \text{and} \quad R(R+1) + R_i < 0,$$

some modes undergo a power law growth, while other undergo a power law decay. When considering one-quarter of circle of radius k_h in the (k_1, k_2) plane, the modes with a power law growth are characterized by $\varphi_n \leq \varphi \leq \pi/2$, while those with a power law decay are characterized by $0 \leq \varphi < \varphi_n$, (see figure 4-c), where

$$\varphi_n = \arcsin \left(\frac{-R_i}{R(R+1)} \right)^{1/2}. \tag{55}$$

For the stable region defined by

$$0 < R_i < 1/4 \quad \text{and} \quad R(R+1) > 0$$

or

$$R(R+1) < 0 < R(R+1) + R_i \quad \text{and} \quad 0 < R_i < 1/4,$$

(i.e., the region (II) in figure 3), some modes undergo a power law decay and other exhibit a "damped oscillatory" behavior. In figure 4(a) the former modes are characterized by $0 \leq \varphi < \varphi_{rs}$, while the later ones are characterized by $\varphi_{rs} < \varphi \leq \pi/2$, where

$$\varphi_{rs} = \arcsin \left(\frac{1 - 4R_i}{(2R+1)^2} \right)^{1/2}, \tag{56}$$

i.e., the angle for which $\mu = -1/2$, or equivalently, $\sigma_\varphi^2 = (\cos^2 \varphi)/4$.

For the region defined by

$$R_i < 0 \quad \text{and} \quad R(R+1) + R_i > 0,$$

(i.e., the region (III) in figure 3), some modes undergo a power law growth, while other undergo a power law decay or exhibit a damped oscillatory behavior. The modes with a

power law growth are characterized by $\varphi_n < \varphi \leq \pi/2$ and those with a power law decay are characterized by $\varphi_{rs} < \varphi < \varphi_n$, and those with a "damped oscillatory" behavior are characterized by $0 \leq \varphi < \varphi_{rs}$ (figure 4(b)).

For the region defined by $R_i < 0$ and $R(R+1) < 0$ (i.e., the region (V) in figure 3) there is an algebraic instability for $0 \leq \varphi < \pi/2$ and an exponential instability at $\varphi = \pi/2$.

When $R_i > 1/4$ (this corresponds to the region (I) in figure 3), $|\lambda_2|$ exhibits a damped oscillatory behavior.

Figure 5 shows the neutral curves, which are described by equation (55), in the (R, φ) plane for $R_i = \pm 0.10$. The results for $R_i = 0.1$ are reported in figure 5(a), while those with $R_i = -0.1$ are reported in figure 5(b). The case $R_i = 0$, i.e., without stratification, is shown in figure 5(c) for comparison. The curve φ_{rs}, which is described by equation (56), is represented by doted lines. As it can expected, the domain for which rotation is destabilizing (i.e., $-1 < R < 0$ and $0 < \varphi \leq \pi/2$) in the absence of stratification (see e.g., Salhi [23]), is reduced in the presence of stable stratification ($0 < R_i < 1/4$, this corresponds to the domain delineated by the concave side of the neutral curve) and completely disappears for $R_i > 1/4$. At $R_i = 1/4$, the curve φ_n reduces to the point $(-1/2, \pi/2)$ and the curve φ_{rs} reduces to the straightline $\varphi_{rs} = 0$. The domain for which rotation is stabilizing ($-\infty < R < -1$ or $0 < R < +\infty$ and $0 < \varphi \leq \pi/2$) is reduced in the presence of unstable stratification ($R_i < 0$). In other words, unstable stratification acts to partially destabilize the stabilizing effects of rotation (see figure 5(b)).

On the other hand, from the analysis of exponential growth presented in the later section, one may easily deduce the dominant contribution for each Fourier mode at late times. When $\sigma_\varphi^2 = R(R+1)\sin^2\varphi + R_i > 0$ with $0 \leq \varphi < \pi/2$, both $|\hat{u}_3|$ (vertical mode) and $|\hat{p}|$ (pressure mode) behave like

$$|\lambda_3| \sim (\tau \cos\varphi)^{-1-\mu} \quad -1/2 < \mu < 0,$$

while $|u^{(2)}|$ (poloidal mode) behaves like

$$|\lambda_2| \sim (\tau \cos\varphi)^{\mu} \quad -1/2 < \mu < 0,$$

and the horizontal $|\hat{u}_i|$ $(i = 1, 2)$, toroidal $|u^{(1)}|$ and buoyancy $|u^{(3)}|$ modes approach a non-zero constant value for long times. This is due to the fact that the expression of these modes involve the particular solution g_{ij}^p which is constant (see equation (41)). This behavior cannot exist when rotation and stratification are not simultaneously present or when the

21

wave vector lies in the plane of the basic shear flow (i.e., $k_2 = 0$, as in the study by Johnson & Gammie [2]).

When $\sigma_\varphi^2 = R(R+1)\sin^2\varphi + R_i < 0$ with $0 \le \varphi < \pi/2$, the modes $|\hat{u}_3|$ and $|\hat{p}|$ behave like

$$|\lambda_3| \sim (\tau\cos\varphi)^{-1-\mu} \quad \mu > 0,$$

while the other modes behave like

$$|\lambda_2| \sim (\tau\cos\varphi)^\mu \quad \mu > 0.$$

This implies that, when $0 < \mu < 1$, both $|\hat{u}_3|$ and $|\hat{p}|$ decay with time while the other components grow with time. Note that this situation can occur in the case of Keplerian disks with modest radial gradients for which $|R_i| \ll 1$. Indeed, when $0 < \mu < 1$, one has $R(1+R) < -R_i < 2\cos^2\varphi$, and hence, $-R_i$ is small for $\cos\varphi \ll 1$.

6.2. "Two-dimensional" energy components

As stressed in Introduction, the formalism used for the stability analysis is directly applicable, with a second order statistical quantity connected to its initial counterpart via a twofold product of basic Green's function. Our main purpose is to compute the evolution of the streamwise "two-dimensional" energy components, which can characterize the role of the $k_1 = 0$ mode in the dynamics of large scales motion, as already indicated.

Three-dimensional spectra

Initial velocity fluctuations are chosen as a sum of Fourier modes, with a given dense energy spectrum, say $E(k)$, and generally isotropic conditions,

$$\hat{R}_{ij}(\boldsymbol{K}, 0) = \frac{E(K)}{4\pi K^2} P_{ij}, \quad P_{ij} = \delta_{ij} - K_i K_j / K^2 \tag{57}$$

where $\hat{R}_{ij} \propto \Re\langle\hat{u}_i^*\hat{u}_j\rangle$ is the second-order velocity correlations, P_{ij} is the conventional transverse projection operator and $\langle\cdot\rangle$ denotes ensemble averaging. In addition, we assume that the initial density fluxes and the initial potential energy are zero, or

$$\Re\left\langle u_0^{(1)*} u_0^{(3)}\right\rangle = \Re\left\langle u_0^{(2)*} u_0^{(3)}\right\rangle = 0, \quad \left\langle u_0^{(3)*} u_0^{(3)}\right\rangle = 0$$

Accordingly, the spectral densities of the toroidal and poloidal contributions to kinetic energy, and the spectral density of the potential energy take the form

$$\hat{R}_{tor}(\boldsymbol{k}, t) = \frac{1}{2} \left\langle u^{(1)^*} u^{(1)} \right\rangle = \frac{E(K)}{8\pi K^2} \left(|g_{11}|^2 + |g_{12}|^2 \right),$$

$$\hat{R}_{pol}(\boldsymbol{k}, t) = \frac{1}{2} \left\langle u^{(2)^*} u^{(2)} \right\rangle = \frac{E(K)}{8\pi K^2} \left(|g_{21}|^2 + |g_{22}|^2 \right),$$

$$\hat{R}_{pot}(\boldsymbol{k}, t) = \frac{R_i}{2} \left\langle u^{(3)^*} u^{(3)} \right\rangle = R_i \frac{E(K)}{8\pi K^2} \left(|g_{31}|^2 + |g_{32}|^2 \right). \tag{58}$$

The spectral density of total kinetic energy, $\hat{R}_{kin} = (1/2)\hat{R}_{ii}$, is the sum of poloidal and toroidal ones, or equivalently, the sum of horizontal and vertical ones,

$$\hat{R}_{kin}(\boldsymbol{k}, t) = \hat{R}_{hor}(\boldsymbol{k}, t) + \hat{R}_{ver}(\boldsymbol{k}, t) = \hat{R}_{tor}(\boldsymbol{k}, t) + \hat{R}_{pol}(\boldsymbol{k}, t)$$

where

$$\hat{R}_{ver}(\boldsymbol{k}, t) = \frac{1}{2} \langle \hat{u}_3^* \hat{u}_3 \rangle = \frac{k_h^2}{k^2} \hat{R}_{pol}(\boldsymbol{k}, t), \tag{59}$$

since $\hat{u}_3 = -(k_h/k)u^{(2)}$.

Streamwise "two-dimensional" kinetic and potential energies

These quantities have been defined in the introduction, eq. (4). The product of the integral length scale $L_{ij}^{(\ell)}$ by related Reynolds stresses represents the limit at $k_\ell = 0$ of the one-dimensional spectrum with respect to the wavenumber k_ℓ, up to a factor π [17]. We will not consider the componentality of $\mathcal{E}_{ij}^{(\ell)}$ here, but only its contribution to kinetic energy, summing up the indices i and j. Accordingly is defined

$$\mathcal{K}L^{(\ell)} = \pi \int_{k_\ell=0} \mathcal{E}_{cin}(k_\ell = 0, t) d^2\boldsymbol{k}. \tag{60}$$

Similarly, the two-dimensional potential energy in the x_ℓ direction takes the form

$$\mathcal{K}_P L_P^{(\ell)} = \pi \int_{k_2=0} \hat{R}_{pot}(k_\ell = 0, t) d^2\boldsymbol{k}, \tag{61}$$

where $\mathcal{K}_P = \int \hat{R}_{pot}(\boldsymbol{k}, t) d\boldsymbol{k}$ and $L_P^{(\ell)}$ is its associated integral length scales in the x_ℓ direction.

Johnson & Gammie [2] considered the spanwise "two-dimensional" energies, and showed analytically that, at large time, $\mathcal{K}L^{(2)} + \mathcal{K}_P L_P^{(2)}$ increasess with time for $R_i < 3/16$ and decreases with time for $R_i > 3/16$ (see their equation (95)). Such an analytical result by [2]

23

holds for the rotating stratified shear case because, at $k_2 = 0$ (so that $\varphi = 0$), the Fourier coefficients do not depend on rotation, as already indicated.

Contrary to the spanwise two-dimensional energies, the streamwise ones, which are related to the $k_1 = 0$ mode, are sensitive to both rotation and stratification. The later ones grow exponentially with time for $R_i + R(R+1) < 0$ and exhibit a damped oscillatory behavior around its limit as $\tau = St \to \infty$ when $R_i + R(R+1) > 0$. For instance, in view of the RDT solution for g_{ij} at $k_1 = 0$ (see Appendix), one shows that

$$\frac{\mathcal{K}L^{(1)}(\tau)}{\mathcal{K}L^{(1)}(0)} = \frac{1}{4\sigma^2} \left[\sigma^2 + \left(R^2 + (1+R)^2\right)\sigma + R^2(R+1)^2 + 2R_i^2\right] +$$

$$\frac{1}{4\sigma^2} \left[\sigma^2 - \left(R^2 + (1+R)^2\right) + R^2(1+R)^2\right] \mathrm{J}_0\left(2\tau\sqrt{\sigma}\right) + \frac{R_iR(1+R)}{\sigma^2}\mathrm{J}_0\left(\tau\sqrt{\sigma}\right), \quad (62)$$

where

$$\mathcal{K}L^{(1)}(0) = \frac{\pi}{2} \int_0^\infty \frac{E(r)}{r}dr, \quad r = \sqrt{k_2^2 + k_3^2},$$

$\sigma = R(1+R) + R_i$ and $\mathrm{J}_0(\tau\sqrt{\sigma})$ is the Bessel function of the first kind of order 0 [29, 30]. In a similar manner, we deduce the evolution of the streamwise two-dimensional potential energy,

$$\frac{\mathcal{K}_P L_P^{(1)}(\tau)}{\mathcal{K}L^{(1)}(0)} = \frac{R_i}{4\sigma^2}\left(\sigma + 3R^2\right) + \frac{R_i}{4\sigma^2}\left(R^2 - \sigma\right)\mathrm{J}_0\left(2\tau\sqrt{\sigma}\right) - \frac{R_iR^2}{\sigma^2}\mathrm{J}_0\left(\tau\sqrt{\sigma}\right). \quad (63)$$

The above relations show that, when $\sigma = R_i + R(1 + R) > 0$, both the streamwise two-dimensional' kinetic and potential energies exhibit a damped oscillatory behavior around the following constant limit:

$$\lim_{\tau \to \infty} \frac{\mathcal{K}L^{(1)}(\tau)}{\mathcal{K}L^{(1)}(0)} = \frac{1}{4\sigma^2}\left[\sigma^2 + \left(R^2 + (1+R)^2\right)\sigma + R^2(R+1)^2 + 2R_i^2\right] \quad (64)$$

$$\lim_{\tau \to \infty} \frac{\mathcal{K}_P L_P^{(1)}(\tau)}{\mathcal{K}L^{(1)}(0)} = \frac{R_i}{4\sigma^2}\left(\sigma + 3R^2\right), \quad (65)$$

because at large time $\tau = St \gg 1$, the Bessel function behaves as [29],

$$\mathrm{J}_0\left(2\tau\sqrt{\sigma}\right) \sim \sqrt{\frac{1}{\tau\sqrt{\sigma}}}\left[\cos\left(2\tau\sqrt{\sigma} - \frac{\pi}{4}\right)\right]. \quad (66)$$

In counterpart, when $\sigma \leq 0$, both $\mathcal{K}L^{(1)}(\tau)$ and $\mathcal{K}_P L_P^{(1)}(\tau)$ grow with time.

24

Long-time behavior of the energy ratio $\eta^{(1)} = \mathcal{K}_P L_P^{(1)}/\mathcal{K}L^{(1)}$

As a preliminar analysis of the relevance of the later analytical results, we consider the long-time limit of the energy ratio $\eta^{(1)} = \mathcal{K}_P L_P^{(1)}/\mathcal{K}L^{(1)}$ in connection to its 3-D counterpart $\eta = \mathcal{K}_P/\mathcal{K}$ which is computed numerically.

When $\sigma = R(1 + R) + R_i > 0$, the Bessel function involving in equations (62)-(63) approaches zero for long times, and hence, one easily deduces the long-time limit of the ratio $\eta^{(1)}$,

$$\eta_\infty^{(1)} = \lim_{\tau \to \infty} \frac{\mathcal{K}_P L_P^{(1)}}{\mathcal{K}L^{(1)}} = \frac{R_i \left(3R^2 + \sigma\right)}{\sigma^2 + (R^2 + (1 + R)^2)\sigma + R^2(1 + R)^2 + 2R_i^2}. \tag{67}$$

Figure 6(a) shows the variation of $\eta_\infty^{(1)}$ versus $-2 \le R \le 1$ at $\sigma = 0.1$, so that, $-1.9 \le R_i = 0.1 - R(1 + R) \le 0.35$. The numerical RDT results for the 3-D energy ratio $\eta = \mathcal{K}_p/\mathcal{K}$ at $\tau = St = 50, 70$ and $\tau = 100$ are also reported in figure 6(a). Obviously, in view of the definition of the potential energy, $\mathcal{K}_p = (1/2)R_i \left\langle u^{(3)} u^{(3)} \right\rangle$, the energy ratios $\eta^{(1)}$ and η are positive when $R_i > 0$, take a zero value at $R_i = 0$ and become negative when $R_i < 0$. As it can be seen, when the long-time limit of η is positive (so that $R_i > 0$ and R ranges between $R_{1,2} = (-1 \pm \sqrt{1.4})/2$, i.e., the roots of the algebraic equation $R(R+1) = \sigma = 0.1$), relation (67) constitutes a good approximation of the variation of η versus R (see also figure 6(b) obtained at $\sigma = 1$). Otherwise (i.e., when $R_i < 0$ with $\sigma > 0$), the long-time limit of η do not exactly follow relation (67) as also shown by figure 6(b). The difference between η and $\eta_\infty^{(1)}$ would be mainly due to the fact that the contribution to the energy ratio η coming from the $k_1 = 0$ mode does not dominate the contribution of the other modes. Indeed, the case where $R_i < 0$ and $\sigma = R(1+R) + R_i > 0$, so that $\sigma_\varphi^2 = R(1+R)\sin^2 \varphi + R_i > 0$, corresponds to the domain (III) in figure 3 in which stable and unstable modes coexist and the $k_1 = 0$ mode is rather stable.

When $\sigma = R(1+R) + R_i \le 0$, the $k_1 = 0$ mode is the most unstable one and the important contribution to the energy ratio η comes from this mode. This can explain the expected agreement between η and $\eta_\infty^{(1)}$ as shown in figures 7(a),(b) displaying the variation of these parameters for $\sigma = 0$ and $\sigma = -0.1$, respectively. At $\sigma = R(1 + R) + R_i > 0$, the long-time limit $\eta_\infty^{(1)}$ is deduced from equations (62) and (63). Indeed, at large time and when $\sigma > 0$, the dominant term in the right hand side of equation (62) (respectively, equation (63)) is

25

the term involving $J_0(2\tau\sqrt{\sigma})$, so that

$$\eta_\infty^{(1)} = \frac{R_i\left(R^2 - \sigma\right)}{\sigma^2 - (R^2 + (1+R)^2)\sigma + R^2(1+R)^2}. \tag{68}$$

At $\sigma = 0$, the solution g_{ij} exhibits an algebraic growth (see equation (73) in Appendix), and one easily obtains the following relation

$$\eta_\infty^{(1)} = -\frac{R}{(1+R)}, \tag{69}$$

which can be also deduced by setting $\sigma = 0$ in relation (68). Relation (69) indicates that for, at large time and when the absolute vorticity vector becomes zero (i.e., $R = -1$ or $S = -2\Omega$), the streamwise "two-dimensional" kinetic energy remains very small with respect to $\mathcal{K}_p L_p^{(1)}$. The numerical RDT results for the energy ratio η at large time show that, near $R = -1$, one also has $|\mathcal{K}_p| \ll \mathcal{K}$ (see figure 7(a) obtained at $\tau = St = 100$).

7. CONCLUDING REMARKS

We have analyzed, using linear theory in the Boussinesq approximation, the stability of an unbounded sheared flow with system rotation around the spanwise (x_2) axis and vertical (x_3) stratification. The base flow is a particular solution of the Euler equations and the base Ertel potential is zero. The conservation of absolute potential vorticity —not new— is considered, and gives here an invariant of the motion for the disturbance field, in which the mean shear vorticity is called into play, in addition to system vorticity: a new important result. Conditions for validity of linearization of the equations for the perturbations were discussed. Plane-wave disturbances with time-dependent wave vector were considered and their governing equations were derived in a local frame attached to the wave vector and in which the incompressibility constraint is satisfied by construction. A linear differential system (with time-dependent coefficients) for the poloidal, toroidal and potential modes is derived. Due to the conservation of the Ertel potential, which leads to a constant of motion relating the toroidal and the potential modes, the rank-three differential system reduces to a rank-two one. In order to consider arbitrary initial conditions and solenoidal property for the velocity field, a reduced Green function **g** has been introduced.

An alternative formulation of the rank-two differential system of equations yields a non-homogeneous second-order differential equation with time-dependent coefficients. An analytical solution has been derived for any orientation of the wave vector and for all values of

26

the rotation R and Richardson R_i numbers. The solution indicates that, for certain cases, all the components of the matrix $\mathbf{g}$ have not the same long-time behavior, so that an analysis in term of exponential growth, as in normal-mode stability analysis, is necessary. This analysis relies only on the *invariants* on the Green function matrix. It is shown that one of the eigenvalues of the matrix $\mathbf{g}$ is unity, reflecting the existence of the linearized Ertel invariant, so that the sum of the two other ones is *trace* $\mathbf{g} - 1$ and their product is K/k, where k is the radial wavenumber at time t and K is its initial value. The determinant of $\mathbf{g}$ is K/k for sheared flows, even for time-dependent sheared flows [10] and with additional effect of rotation and stratification. Therefore the normal-mode stability analysis lies on *trace* $\mathbf{g}$ as the unique unknown to be calculated, and its long-time behavior was analyzed in terms of the rotation number, of the Richardson number, and of the azimutal angle φ. It is shown that the flow stability is governed by the parameter $\sigma_\varphi^2 = R(1+R)\sin^2\varphi + R_i$. The modes for which $\sigma_\varphi^2 > 0$ are stable, those for which $\sigma_\varphi^2 = 0$ are neutral, while those for which $\sigma_\varphi^2 < 0$ are unstable. In their linear stability analysis of accretion disks, Johnson & Gammie [2] have only considered the case where $\varphi = 0$ (i.e., the $k_2 = 0$ mode) for which rotation effects vanish.

It is shown now that, when $\sigma_\varphi^2 < 0$ (unstable case), the particular value $\varphi = \pi/2$ (i.e., the $k_1 = 0$ mode) corresponds to the most unstable mode for which the solution exhibits an exponential growth, while the other unstable modes are characterized by an algebraic growth. An algebraic growth is found for the neutral modes (i.e., those characterized by $\sigma_\varphi^2 = 0$). The stable modes (i.e., those characterized by $\sigma_\varphi^2 > 0$) undergoe a power law decay if $0 < \sigma_\varphi^2 < (\cos^2\varphi)/4$ or exhibit a damped oscillatory behavior if $\sigma_\varphi^2 > (\cos^2\varphi)/4$.

For geophysical and astrophysical applications, stability diagrams have been plotted for all values of the Richardson and rotation numbers. For instance, in the $(R(1+R), R_i)$ plane, five domains have been distinguished. In the $R_i > 1/4$ domain (i.e., the domain (I) in figure 2), the modes are stable exhibiting a damped oscillatory behavior. In the domain corresponding to $R_i < 0$ and $R(1+R) < 0$ or $R(R+1) < 0 < R(R+1)+R_i$ and $0 < R_i < 1/4$ (i.e., the domain (II) in figure 2), the modes are also stable but there are ones exhibiting a damped oscillatory behavior while the other undergo a power law decay. In the $R_i < 0$ and $R(R+1) < 0$ domain (i.e., the domain (V) in figure 2), the modes are unstable. In the other two domains (i.e., the domains (III) and (IV), see figure 2) stable and unstable modes can coexist.

Because previous DNS studies for sheared homogeneous turbulence at high initial shear rate show that the linear theory contains the essential mechanism responsible for development of turbulence structures, and the region near the $k_1 = 0$ mode has an important implication on the dynamics of large scales motion, the formalism used for the RDT-like stability analysis is systhematically applied to compute the evolution of particular turbulence statistics: the streamwise "two-dimensional" kinetic and potential energies. It is shown that the long-time limit of the ratio, denoted by $\eta_\infty^{(1)}$ of these two-dimensional energies (potential over kinetic) depends on both rotation and stratification. As a preliminar evaluation of the relevance of the computation of the streamwise two-dimensional energy components, the variation of $\eta_\infty^{(1)}$ versus R or R_i for fixed values of $\sigma = R(1 + R) + R_i$ has been compared to the long-time limit of that one of its three-dimensional counterpart, denoted by η, computed numerically. The conclusion that can be drawn from this comparison is that, when the couple $(R(R(1 + R), R_i)$ lies in the domain (III) of the diagram shown in figure 2, the contribution coming from the $k_1 = 0$ is not a dominant one in the evolution of energies. At least, this point shows the usefulness of a complete stability analysis as the one presentend in this study.

On the other hand, because in many accretion disks angular momentum is likely redistributed internally by MHD turbulence driven by magnetorotational instability (see Balbus & Hawley [31]), it appears very useful for astrophysical applications to study, in a subsequent paper, the effects of a magnetic field on stratified rotating sheared turbulence. Finally, this linear study may pave the way for a fully nonlinear one using pseudo-spectral DNS in terms of comoving deformed coordinates [32].

Appendix

Equations for the poloidal, toroidal and potential modes

By using the expression of the pressure mode $\hat{p}$ given by equation (15), the equations for the modes $\hat{u}_i$ and $\hat{b}$ given by system (16) can be rewritten as

$$\frac{d\hat{u}_i}{dt} + \mathcal{L}_{ij}\hat{u}_j = \left(\delta_{i3} - \frac{k_i k_3}{k^2}\right)\hat{b}, \quad \frac{d}{dt}\hat{b} = -N^2\hat{u}_3, \quad k_i\hat{u}_i = 0, \tag{70}$$

with

$$\mathcal{L}_{ij} = S\left(\delta_{i1} - 2\frac{k_i k_1}{k^2}\right)\delta_{j3} + 2\Omega\left(\delta_{in} - \frac{k_i k_n}{k^2}\right)\epsilon_{n2j}. \tag{71}$$

The substitution of the relation $\hat{u}_i = u^{(\alpha)} e_i^{(\alpha)}$ where $(i = 1, 2, 3)$, $(\alpha = 1, 2)$, into the first equation in (70) implies

$$\frac{du^{(\beta)}}{dt} + u^{(\alpha)}\left[e_i^{(\beta)}\frac{de_i^{(\alpha)}}{dt}\right] + e_i^{(\beta)}\left(S\delta_{i1}\delta_{j3} + 2\Omega\epsilon_{i2j}\right)e_j^{(\alpha)}u^{(\alpha)} = \hat{b}e_i^{(\beta)}\delta_{i3}.$$

Because the local frame $(\boldsymbol{e}^{(1)}, \boldsymbol{e}^{(2)}, \boldsymbol{e}^{(3)})$ is an orthonormal one and $\boldsymbol{e}^{(1)}$ is time-independent, then

$$\left[e_i^{(\beta)}\frac{de_i^{(\alpha)}}{dt}\right] = 0, \quad (\alpha, \beta = 1, 2), \ (i = 1, 2, 3).$$

Therefore, the equations for $u^{(1)}$, $u^{(2)}$ and $u^{(3)} = -\hat{b}/N$ can be rewritten as

$$\frac{du^{(\beta)}}{dt} + \left[e_i^{(\beta)}\left(S\delta_{i1}\delta_{j3} + 2\Omega\epsilon_{i2j}\right)e_j^{(\alpha)}\right]u^{(\alpha)} + \left[Ne_i^{(\beta)}\delta_{i3}\right]u^{(3)} = 0,$$

$$\frac{du^{(3)}}{dt} - \left[Ne_i^{(\beta)}\delta_{i3}\right]u^{(\beta)} = 0, \quad (\alpha, \beta = 1, 2), \ (i = 1, 2, 3),$$

that are equivalent to system (20).

Solution for the reduced Green function

When $\sigma_\varphi^2 \neq 0$, we consider the second-order differential equation for g_{3i} (see equation (38)) which has the particular solution g_{3i}^p given by equation (41). To resolve the associated homogeneous equation we distinguish the case where $k_1 = 0$ (i.e., $\varphi = \pi/2$ and the case where $k_1 \neq 0$.

Case where $k_1 = 0$

When $\xi^2 = \sigma\left(k_h^2/k^2\right) > 0$ with $k_2/k > 0$, the solution of equation (38) is found as

$$g_{11} = 1 - \frac{R(1+R)}{\sigma}\left(1 - \cos\xi\tau\right), \quad g_{12} = \frac{(1+R)}{\sqrt{\sigma}}\sin\xi\tau,$$

$$g_{13} = \frac{R_i\left(R+1\right)}{\sigma}\left(1 - \cos\xi\tau\right), \quad g_{21} = -\frac{R}{\sqrt{\sigma}}\sin\xi\tau,$$

$$g_{22} = \cos\xi\tau, \quad g_{23} = \frac{R_i}{\sqrt{\sigma}}\sin\xi\tau, \quad g_{31} = \frac{R}{\sigma}\left(1 - \cos\xi\tau\right)$$

29

$$g_{32} = -\frac{1}{\sqrt{\sigma}} \sin \xi\tau, \quad g_{33} = 1 - \frac{R_i}{\sigma}(1 - \cos \xi\tau) \tag{72}$$

Recall that $\sigma = R(1 + R) + R_i$. The solution corresponding to $\xi^2 = \sigma k_h^2/k^2 < 0$, can be deduced from the above one by using the basic functional relations $\sinh x = -\imath \sin(\imath x)$ and $\cosh x = \cos(\imath x)$. In that case, the solution exhibit an exponential growth. As for the solution associated to the case where $\sigma = R(1 + R) + R_i = 0$, it can also be deduced from the later solution,

$$g_{11} = 1 - R(1 + R)\frac{k_2^2}{k^2}\frac{\tau^2}{2}, \quad g_{12} = (1 + R)\frac{k_2}{k}\tau,$$

$$g_{13} = R_i(1 + R)\frac{k_2^2}{k^2}\frac{\tau^2}{2}, \quad g_{21} = -R\frac{k_2}{k}\tau, \quad g_{22} = 1$$

$$g_{23} = R\frac{k_2}{k}\tau, \quad g_{31} = R\frac{k_2^2}{k^2}\frac{\tau^2}{2},$$

$$g_{32} = -R\frac{k_2}{k}\tau, \quad g_{33} = 1 + R(1 + R)\frac{k_2^2}{k^2}\frac{\tau^2}{2}. \tag{73}$$

Therefore, at $\sigma = 0$, the solution exhibits an algebraic growth.

Case where $k_1 \neq 0$.

At $k_1 \neq 0$, the homogeneous equation associated to (38) is tansformed (by using the pure imaginary variable $z = \imath k_3/k_h$) to equation (43) with solution $g_{3j} = C_{0j}P_\mu(z) + C_{1j}Q_\mu(z)$. So that, the solution of the non-homogeneous equation (38) can be written

$$g_{3j} = C_{0j}P_\mu(z) + C_{1j}Q_\mu(z) + g_{3j}^p \quad (j = 1, 2, 3), \tag{74}$$

and, in view of equation (32) that can be rewritten as

$$g_{2j} = \left(-\imath\sqrt{1 - z^2}\cos\varphi\right)\frac{dg_{3j}}{dz},$$

we obtain

$$g_{2j} = (-\imath\cos\varphi)\sqrt{1 - z^2}\left[C_{0j}P'_\mu(z) + C_{1j}Q'_\mu(z)\right], \tag{75}$$

while, equation (29) allows us to determine g_{1j},

$$g_{1j} = \delta_{1j} + (R\sin\varphi)(\delta_{3j} - g_{3j}),$$

$$g_{1j} = \delta_{1j} + (R\sin\varphi)\left[\delta_{3j} - C_{0j}P_\mu(z) - C_{1j}Q_\mu(z) - g_{3j}^p\right]. \tag{76}$$

30

Here, g_{3j}^p is given by equation (41), and C_{0j} and C_{1j} are constants that can be determined by using the initial conditions, $g_{ij}(z_0) = \delta_{ij}$. The result is

$$C_{0j} = \left(1 - z_0^2\right)\left[\left(\delta_{3j} - g_{3j}^p\right)Q_\mu'(z_0) + \frac{\imath}{\cos\varphi}\frac{Q_\mu(z_0)}{\sqrt{1 - z_0^2}}\delta_{2j}\right],$$

$$C_{1j} = -\left(1 - z_0^2\right)\left[\frac{\imath}{\cos\varphi}\frac{P_\mu(z_0)}{\sqrt{1 - z_0^2}}\delta_{2j} + \left(\delta_{3j} - g_{3j}^p\right)P_\mu'(z_0)\right].$$

It follows that

$$g_{11} = 1 - g_{33}^p\left[1 - \left(1 - z_0^2\right)\left[Q_\mu'(z_0)P_\mu(z) - P_\mu'(z_0)Q_\mu(z)\right]\right],$$

$$g_{33} = \left(1 - z_0^2\right)\left[Q_\mu'(z_0)P_\mu(z) - P_\mu'(z_0)Q_\mu(z)\right] + \left[1 - \left(1 - z_0^2\right)\left[Q_\mu'(z_0)P_\mu(z) - P_\mu'(z_0)Q_\mu(z)\right]\right]g_{33}^p,$$

$$g_{22} = \left(1 - z_0^2\right)\left(\frac{1 - z^2}{1 - z_0^2}\right)^{1/2}\left[P_\mu(z_0)Q_\mu'(z) - Q_\mu(z_0)P_\mu'(z)\right].$$

Therefore, *trace* **g** is independent on the particular solution g_{ij}^p.

---

[1] J. Pedlowski, *Geophysical Fluid dynamics*, 2nd Ed., Springer. (1986).

[2] B.M. Johnson & C.F. Gammie, *ApJ*, **626**, 978 (2005).

[3] B.J. Bayly, *Phys. Rev. Lett.* **57**, 2160 (1986).

[4] A.D.D. Craik, *J. Fluid Mech.*, **198**, 275 (1989).

[5] J. W. Miles, *J. Fluid Mech.*, **10**, 496 (1961).

[6] P.G. Drazin & W.H. Reid, *Hydrodynamic stability*, CUP (1981).

[7] T. Miyazaki, *Phys. Fluids A* **5**, 2702 (1993).

[8] C. Cambon, J-P Benoit, L. Shao & L. Jacquin, *J. Fluid Mech.*, **278**, 175–200 (1994).

[9] R.R. Kerswell, *Ann. Rev. Fluid Mech.* **34**, 83 (2002).

[10] A. Salhi & C. Cambon, *Phys. Rev.* E, **75**, 016312 (2007).

[11] A. Salhi & C. Cambon, *Phys. Rev.* E, **79**, 036303 (2009).

[12] I. Rogachevskii & N. Kleeorin, *Phys. Rev.* E, **68**, 036301 (2003).

[13] N. Leprovost & E.-J. Kim, Phys. Rev. E **78**, 016301 (2008).

[14] H.K. Moffatt, "The interaction of turbulence with strong wind shear," Colloquium On Atmospheric Turbulence and Radio Wave Propagation. (ed., A.M. Yaglom & V.I. Tatarsky), Nauka, Moscow, 139 (1967).

[15] L. J. A. van Bockhoven *et al.*, *Journal of Turbulence*, **9**, 1–24 (2008).

[16] P. Sagaut & C. Cambon, *Homogeneous turbulence dynamics.* CUP (2008).

[17] A. Salhi & C. Cambon, *J. Fluid Mech.* **347**, 171 (1997).

[18] H. Hanazaki & J.C.R. Hunt, *J. Fluid Mech.* **507**, 1 (2004).

[19] S.C. Kassinos, E. Akylas & C.A. Langer, *Phys. Fluids* **19**, 021701 (2007).

[20] H.P. Greenspan, *The theory of Rotating Fluids.* CUP (1968).

[21] G. K. Batchelor & I. Proudman, *Q. J. Mech. Appl. Math.* **7**, 83 (1954).

[22] A.A. Townsend, *The structure of turbulent shear flow* . CUP (1976).

[23] A. Salhi, *Theor. Comp. Fluid Dyn.* **15**, 339 (2002).

[24] R. T. Pierrehumbert, *Phys. Rev. Lett.* **57**, 2157 1986.

[25] J.M. Lee, J. Kim & P. Moin, *J. Fluid Mech.* **216**, 561 (1990).

[26] F.G. Jacobitz & S. Sarkar, *Theor. Comp. Fluid Dyn.* **13**, 171 (1999).

[27] G. Brethouwer, *J. Fluid Mech.* **542**, 305 (2005).

[28] L. M. Smith & F. Waleffe, *J. Fluid Mech.* **451**, 145 (2002).

[29] I. S. Gradshteyn, & I.M. Ryzhik, *Table of Integrals, Series, and Products.* Academic Press. (1965).

[30] A. Erdelyi, W. Magnus, F. Oberhettinger & F. G. Tricomi, *Higher Transcendental Functions.* McGraw-Hill, New York, Vol. 1-3 (1953).

[31] S.A. Balbus & J. F. Hawley, *ApJ*, **467**, 76 (1998).
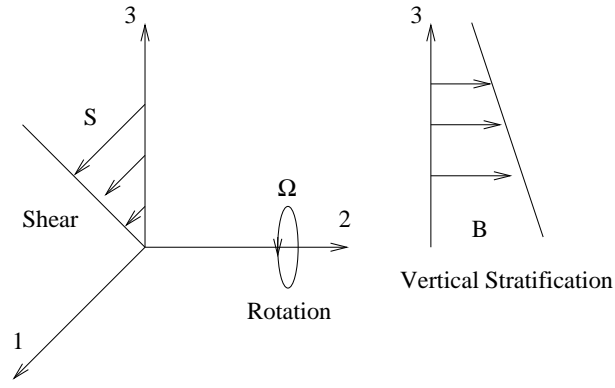
[32] R. Rogallo, NASA Tech. Memo. No. 81315 (1981).

FIG. 1: Rotating stratified shear flow: $U_i = Sx_3\delta_{i1}$ (Shear), $\Omega_i = \Omega\delta_{i2}$ (Rotation), $B = N^2x_3$ (Vertical stratification).
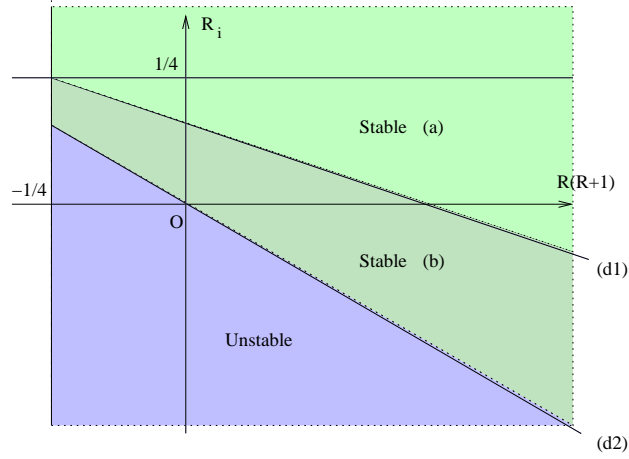

FIG. 2: Stability diagram in the $(R(R+1), R_i)$ plane for given values of φ_n (see Eq. (55)) and $\varphi_{rs} < \varphi_n$ (see Eq. (56)).

(d1): $R_i = -R(R+1)\sin^2\varphi_{rs} + (\cos^2\varphi_{rs})/4$. (d2): $R_i = -R(R+1)\sin^2\varphi_n$.

Stable (a): damped oscillatory behavior, $|\lambda_2|^2 \sim e^{-y}[A + r_0\cos(\Im\mu y + \beta)]$ with $y = \log(\tau\cos\varphi)$.

Stable (b): power law decay, $|\lambda_2| \sim (\tau\cos\varphi)^\mu$ with $-1/2 < \mu < 0$.
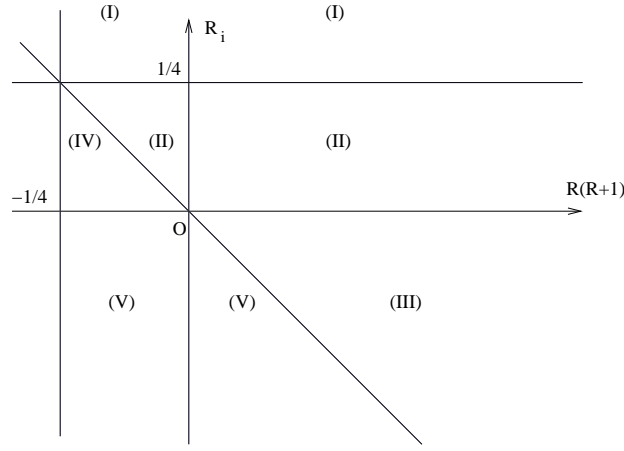
FIG. 3: Stability diagram in the $(R(R+1), R_i)$ plane.

(I): $R_i > 1/4$. Region with stable modes exhibiting a damped oscillatory behavior.

(II): $0 < R_i < 1/4$ and $R(R+1) > 0$ or $R(R+1) < 0 < R(R+1) + R_i$ and $0 < R_i < 1/4$. Region with stable modes in which modes with damped oscillatory behavior and modes with power law decay can coexist.

(III): $R_i < 0 < R(R+1) + R_i$. Stable ((a),(b)) and unstable modes can coexist.

(IV): $0 < R_i < 1/4$ and $R(R+1) < R(R+1) + R_i < 0$. Stable (b) and unstable modes can coexist.

(V): $R_i < 0$ and $R(R+1) + R_i < 0$. Region with unstable modes.
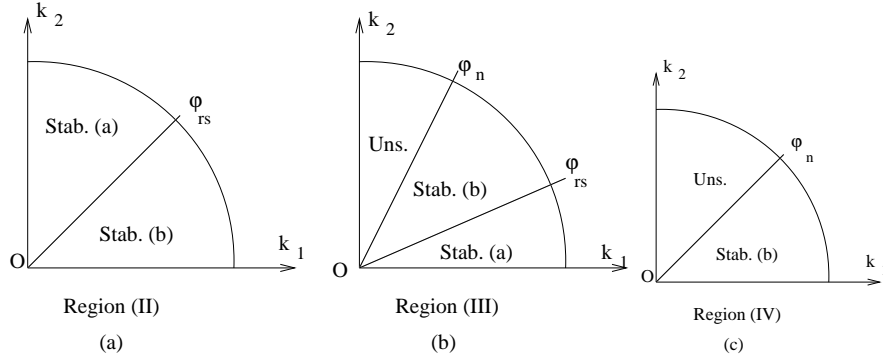
FIG. 4: Stability diagram in the (k_1, k_2) plane.

(a) Region (II); (b) Region (III); (c) Region (IV) defined in figure 2. φ_n and φ_{rs} are defined by equations (55) and (56), respectively.
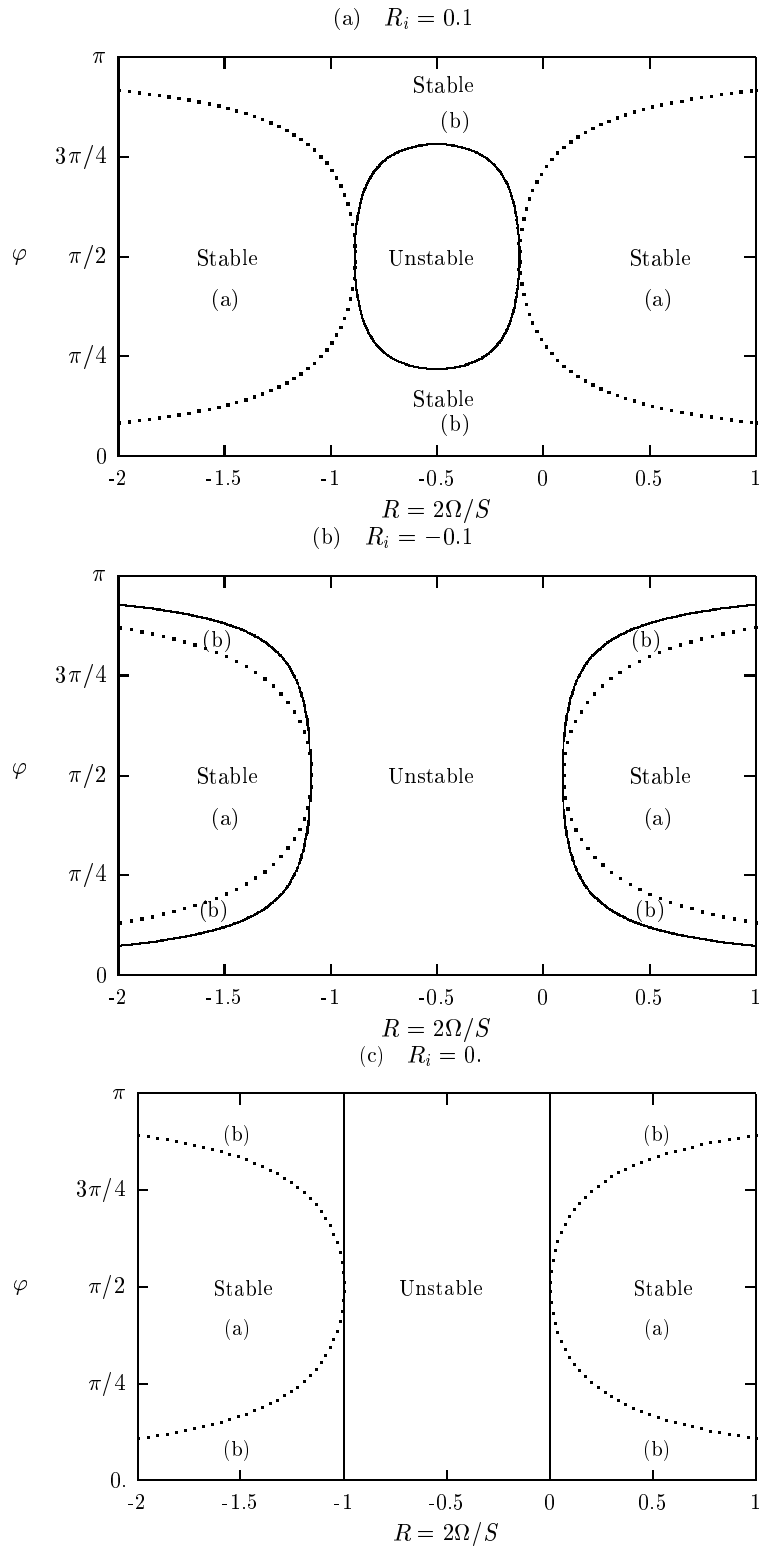
(a) $R_i = 0.1$

(b) $R_i = -0.1$

(c) $R_i = 0.$

FIG. 5: Stability diagram in the (R, φ) plane. φ_{rs} given by equation (56) is represented by doted lines.   (a) $R_i = 0.1$, (b) $R_i = -0.1$, (c) $R_i = 0$.
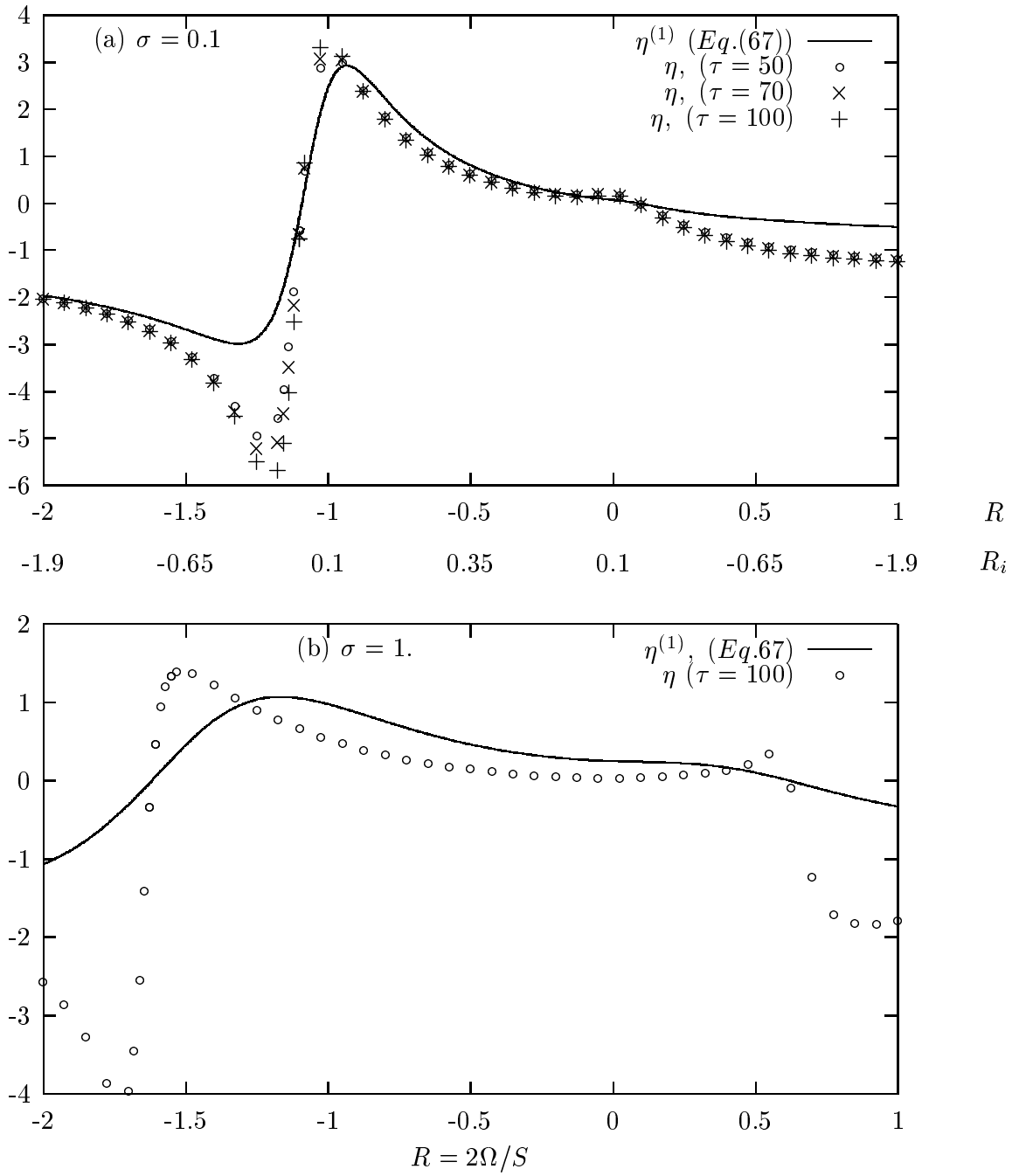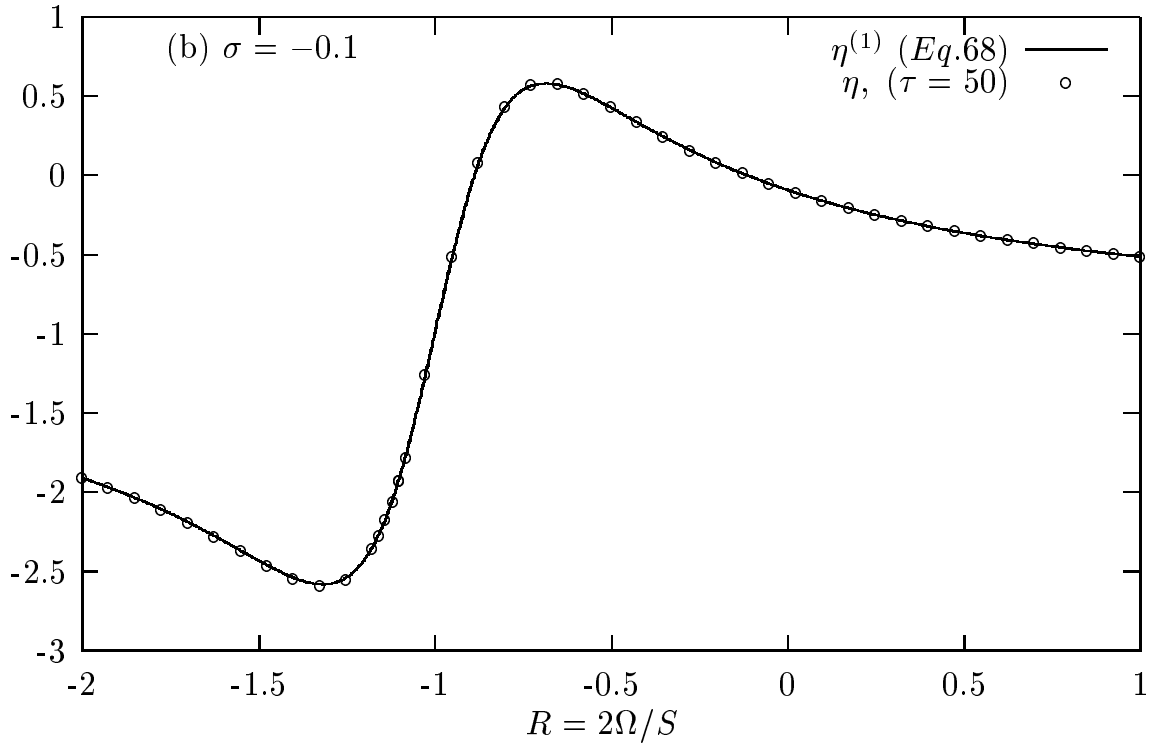
35

FIG. 6: Variation of the long-time limit of the "two-dimensional" energy ratio, $\eta^{(1)} = \mathcal{K}_p L_p^{(1)}/\mathcal{K}L^{(1)}$ (equation (67)) and its 3-D counterpart $\eta = \mathcal{K}_p/\mathcal{K}$ versus the rotation number R for a fixed positive value of $\sigma = R(1+R) + R_i$. (a) $\sigma = 0.1$, (b) $\sigma = 1$.
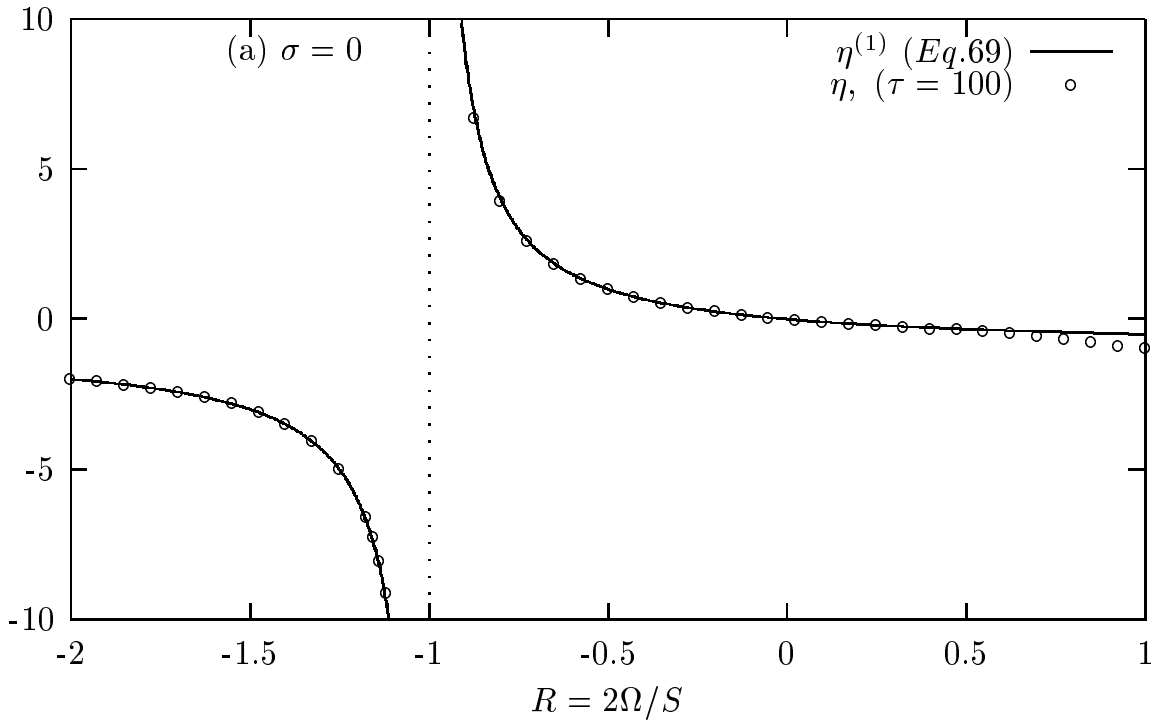
FIG. 7: Variation of the long-time limit of the "two-dimensional" energy ratio, $\eta^{(1)} = \mathcal{K}_p L_p^{(1)}/\mathcal{K}L^{(1)}$ (equations (68)-(69)) and its 3-D counterpart $\eta = \mathcal{K}_p/\mathcal{K}$ versus the rotation number R for a fixed value of $\sigma = R(1+R) + R_i$. (a) $\sigma = 0.0$, (b) $\sigma = -0.1$